iScience

CellPress
OPEN ACCESS

Article

MiR-203 is an anti-obese microRNA by targeting apical sodium-dependent bile acid transporter

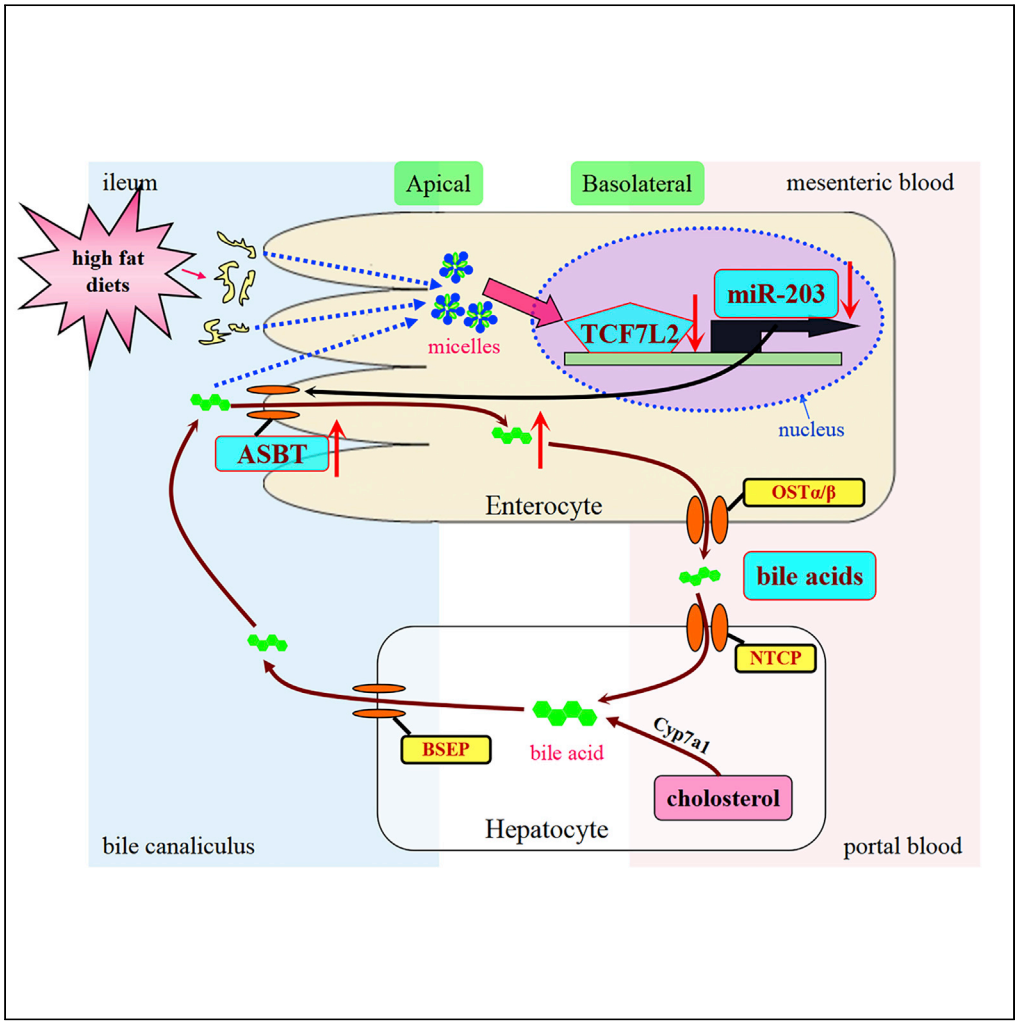

Xin Liu, Feiran Cheng, Xue Bai, ..., Ning Ma, Baofeng Yang, Yong Zhang

yangbf@ems.hrbmu.edu.cn (B.Y.)
hmuzhangyong@hotmail.com (Y.Z.)

Highlights

miR-203 is downregulated in obese rodents and overweight/obese population

ASBT is a direct target of miR-203 in obesity

TCF7L2 acts as an upstream activator of miR-203 in obesity

miR-203 ameliorates obesity and dyslipidemia by increasing TBAs and lipids excretion

Liu et al., iScience 25, 104708
August 19, 2022
https://doi.org/10.1016/j.isci.2022.104708

iScience

CellPress
OPEN ACCESS

Article

MiR-203 is an anti-obese microRNA by targeting apical sodium-dependent bile acid transporter

Xin Liu,[1,3] Feiran Cheng,[1] Xue Bai,[1] Tong Zhao,[1] Limin Zhao,[1] Lei Wang,[1] Mingqi Li,[1] Xianxian Wu,[1] Xiaohui Chen,[1] Pingping Tang,[1] Mengxue Wang,[1] Lintong Jiang,[1] Chaoqi Yan,[5] Fenghua Pei,[6] Xu Gao,[7] Ning Ma,[7] Baofeng Yang,[1,2,3,*] and Yong Zhang[1,3,4,8,*]

SUMMARY

Obesity is characterized by excessive fat deposition within the body. Bile acids (BA) are important regulators for controlling the absorption of lipid. Here we show that miR-203 exerts weight-loss and lipid-lowering effects by increasing total BA excretion in obese rodents. miR-203 overexpression transgenic mice are resistant to high-fat diet (HFD)-induced obesity and dyslipidemia. Moreover, the knockdown of miR-203 deteriorates metabolic disorders. ASBT plays important role in regulating BA homeostasis and is a direct target of miR-203. In human intestinal epithelial cells, overexpression of miR-203 decreases the cellular uptake of BA by inhibiting ASBT. Furthermore, TCF7L2 is downregulated in obese mice and acts as a transcription factor of miR-203. The ASBT mRNA level was positively correlated with the body mass index (BMI) of population, while the miR-203 level was negatively associated with BMI. Taken together, these data suggest miR-203 could be a new therapeutic BA regulator for obesity and dyslipidemia.

INTRODUCTION

Obesity is a serious public health threat that increases the morbidity and mortality of diseases, including metabolic disorders, cardiovascular diseases, and cancers (Wang et al., 2021). The prevalence of childhood and adult obesity has almost tripled in the past four decades, which impairs people's health and health-related quality of life (Lingvay et al., 2021). According to the latest data from the NCD Risk Factor Collaboration, almost 39% (2 billion) of the adult population were overweight globally with a body mass index (BMI) of $\geq$25 kg/m^2. 12% (671 million) of the adult population were considered obesity (BMI $\geq$30 kg/m^2), which was triple since 1975. It is expected that the proportion of obesity will increase to 20% of the world population by 2025 (Tysoe, 2021). The lack of more effective anti-obesity therapies highlights the need to deeply investigate the physiopathology of obesity so as to identify novel therapeutic targets and develop effective therapeutic strategies.

On average, 40% or more of the daily energy requirement in humans is supplied by dietary fats (Yang et al., 2021). Bile acid (BA) is responsible for assisting the formation of the micelles in intestine, which promotes the degradation and elimination of exogeneous dietary fat in the body (Castellanos-Jankiewicz et al., 2021). Owing to the novel roles of BA in lipid metabolism and homeostasis, decreasing BA content and modulating BA composition to regulate BA signaling are novel directions for developing therapeutic strategies for obesity. Additionally, BA functions as signaling molecules that participate multiple signaling pathways in various physiopathological conditions, and thus, regulating lipid homeostasis.

ASBT, apical sodium-dependent BA transporter playing a critical role in maintaining BA homeostasis, is normally expressed in the brush border of the terminal ileum, and its expression is remarkably increased in obesity (Ovadia et al., 2019) (Li et al., 2020). The important role of ASBT in BA reabsorption from small intestine makes it an attractive target for therapeutic intervention in BA-related diseases including obesity and related metabolic disorders (Poupon, 2016). There are several candidate inhibitors of ASBT in the drug development pipeline and some of them have advanced into clinical trials, such as Elobixibat, Volixibat, and Linerixibat for the treatment of chronic idiopathic constipation (CIC), type 2 diabetes (T2D) and primary biliary cholangitis (PBC) (Nakajima et al., 2018; Poupon, 2016). However, therapeutic prodrugs targeting ASBT were less progressed to market owing to the challenges of thorough understanding of the

[1]Department of Pharmacology (the State-Province Key Laboratories of Biomedicine-Pharmaceutics of China, Key Laboratory of Cardiovascular Research, Ministry of Education), College of Pharmacy, Harbin Medical University, Harbin 150081, China

[2]Department of Pharmacology and Therapeutics, Melbourne School of Biomedical Sciences, Faculty of Medicine, Dentistry and Health Sciences University of Melbourne, Melbourne, VIC 3010, Australia

[3]Research Unit of Noninfectious Chronic Diseases in Frigid Zone, Chinese Academy of Medical Sciences, 2019RU070, Harbin 150081, China

[4]Institute of Metabolic Disease, Heilongjiang Academy of Medical Science, Harbin 150081, China

[5]Department of Breast Surgery, The Second Affiliated Hospital of Harbin Medical University, Harbin 150081, China

[6]Department of Gastroenterology, The Second Affiliated Hospital of Harbin Medical University, Harbin 150081, China

[7]Department of Biochemistry, College of Basic Medicine, Harbin Medical University, Harbin 150081, China

[8]Lead contact

*Correspondence: yangbf@ems.hrbmu.edu.cn (B.Y.), hmuzhangyong@hotmail.com (Y.Z.)

https://doi.org/10.1016/j.isci.2022.104708

complicated biological mechanisms of ASBT. Thus, more studies were necessary in order to reveal and promote anti-ASBT therapy for obesity in view of its important role in maintaining lipid homeostasis.

MicroRNAs (miRNAs) are a class of endogenous non-coding RNAs, on average about 22 nucleotides in length, which exert effects on post-transcriptional gene silencing by binding to complementary sequences in the 3′-untranslated regions (3′UTRs) of target mRNAs (Li et al., 2021a). Plenty of molecular processes are regulated by miRNAs, such as cell cycles, growth, and development (He et al., 2021; Laanesoo et al., 2021). The expression of miRNAs is regulated by many transcription factors. Many classical superfamilies of transcription factors have been proved to be involved in the regulation of miRNAs expression, such as E2F1, MyoD, SRF, and C/EBP alpha (Grimaldi et al., 2021; Treiber et al., 2019). MicroRNA-203 (miR-203) has been identified as a novel regulator in tumor and neurodegenerative diseases (Hur et al., 2017; Swarup et al., 2019). Some studies also revealed that miR-203 were participated in metabolic adaptations of adipose tissue, owing to its promotion effects on white adipose tissue browning and brown adipocyte differentiation (Brandão et al., 2020) (Guo et al., 2019) (Kim et al., 2014). In the current study, we firstly found that miR-203 could complementarily bind with 3′UTR of SLC10A2 (the gene encoding ASBT); however, whether miR-203 is involved in the regulation of BA homeostasis and obesity through targeting ASBT remains unclear.

Here we show that miR-203 controls obesity and dyslipidemia by repressing ASBT expression, which contributes to increased BA and lipid excretion. We also found that TCF7L2 (transcription factor 7-like 2) could regulate miR-203 as its positive transcription factor, which was expressed abundantly in intestinal L cells and has been proved to be related to diabetes and obesity.

RESULTS

miR-203 and apical sodium-dependent bile acid transporter are dysregulated in obese rats

We first developed a rat model of obesity with high-fat diet (HFD) and characterized the biochemical anomalies of obese rats. As illustrated in Figure 1A, obese rats had greater body weight than lean control rats. Expectedly, serum concentrations of triglyceride (TG), total cholesterol (TCH), and low-density lipoprotein (LDL) were significantly higher, whereas high-density lipoprotein (HDL) was lower, in obese rats than in the control counterparts (Figures 1B–1E). Coincidently, a similar increase in the serum level of total BA was seen in the obesity group, but not in the control group (Figure 1F). We then moved forward to see how BA is altered. ASBT is expressed in terminal ileum that transports BAs with high efficiency (Li et al., 2020). Inhibition of ASBT expression or transport activity results in the blockage of enterohepatic circulation of BA with alterations in lipid and BA homeostasis (Newsome et al., 2020). We found that ASBT expression was elevated in ileal RNA and protein samples of obese rats (Figures 1G and 1H). In an effort to search miRNAs with the potential of regulating the pathological process relevant to diet-induced obesity, we identified miR-203 as a possible regulator of ASBT expression through target prediction by Targetscan and microRNA.org databases (Figure S1). In support of this possibility, we found that miR-203 expression was markedly decreased in RNA samples from terminal ileum and serum of obese rats (Figures 1I and 1J).

AgomiR-203 reduces body weight and ameliorates dyslipidemia in obese rats

To test whether miR-203 could be a new therapeutic target to treat obesity, agomiR-203 or its inhibitor antagomiR-203 were utilized. We delivered agomiR-203 and antagomiR-203, as well as mismatched nucleotides as a negative control (NC), into obese rats through intraperitoneal injection. Administration of agomiR-203 significantly elevated miR-203 in terminal ileum (Figure 2A), produced a significant decrease of ASBT expression in mRNA (Figure 2B) and protein levels (Figure 2C) compared to the NC group. In sharp contrast, antagomiR-203 treatment downregulated miR-203 expression and increased ASBT mRNA and protein levels. Moreover, immunofluorescent staining of ASBT protein in mice ileum also indicated the downregulation of ASBT expression in brush border by agomiR-203, whereas increased by antagomiR-203 (Figure 2D). Obese rats with NC treatment developed obesity (Figures 2E and 2F), bulky fat deposition (Figure 2G), and elevated blood lipids (Figures 2H–2K). These disorders were effectively reversed by pretreatment with agomiR-203. However, antagomiR-203 pretreatment increased the body weight and blood lipids compared to NC rats because of the effects of the reduction of nature mature miR-203 which was obviously attributed to the opposite effect of agomiR-203 (Figures 2E–2K). More importantly, to test the alterations of enterohepatic circulation in rats after medicine injection in different groups, concentrations of serum and fecal total BA were measured. AgomiR-203 pretreatment decreased serum BA relative to the values for the NC group which reflected the availability of agomiR-203 and the experimental condition

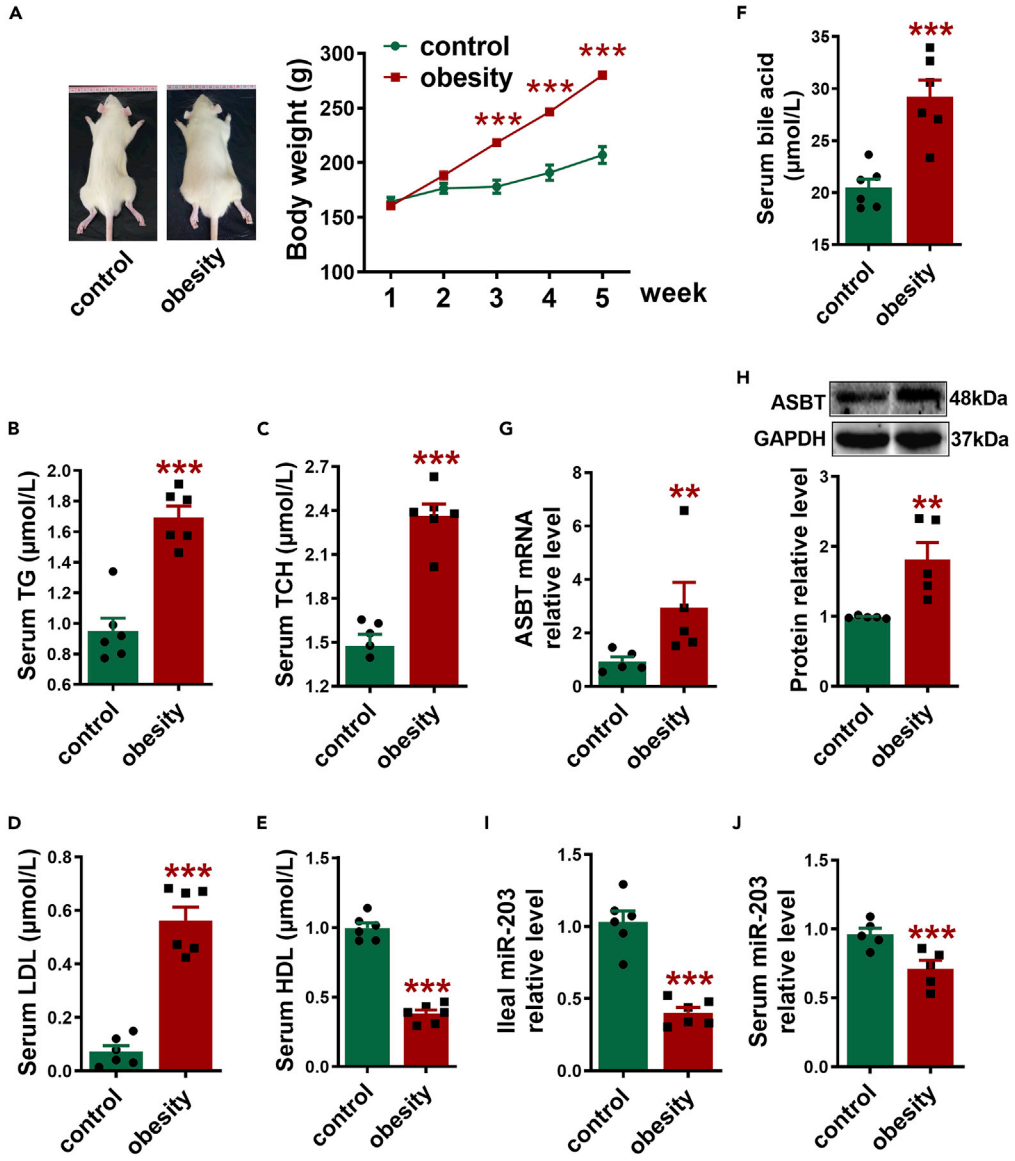

Figure 1. The level of miR-203 decreases and the expression of ASBT increases in obese rats

(A) Comparison of body weight between control and obese rats. Obesity was established in rats subject to a high-fat diet for 4 weeks, body weight of control and obese rats were recorded, n = 6.

(B–E) Serum (B) TG, n = 6, (C) TCH, n = 5, (D) LDL-C, n = 6, and (E) HDL-C levels in control and obese rats were measured, n = 6.

(F) Serum total bile acid levels in control and obese rats were detected, n = 6.

(G and H) The mRNA (G) and protein (H) levels of ASBT in the ileums of control and obese rats were determined by qRT-PCR and Western blot, respectively, n = 5.

(I and J) miR-203 expression levels in the terminal ileum, n = 6 (I) and serum, n = 5 (J) of control and obese rats were determined by qRT-PCR, respectively. The data are expressed as mean ± SEM, **p < 0.01, ***p < 0.001 vs control by Student's t-test.

(Figure 2L). Meanwhile, more BA excretion was observed in feces of agomiR-203 treated rats compared to NC rats; however, antagomiR-203 treatment exerted the opposite results (Figure 2M).

miR-203 inhibits apical sodium-dependent bile acid transporter expression by binding to its 3′UTR

We then tested the inhibitory effect of miR-203 on ASBT. The complementary sequences between miR-203 and 3′UTRs of SLC10A2 are shown in Figure 3A. Luciferase reporter plasmid containing the 3′UTR of

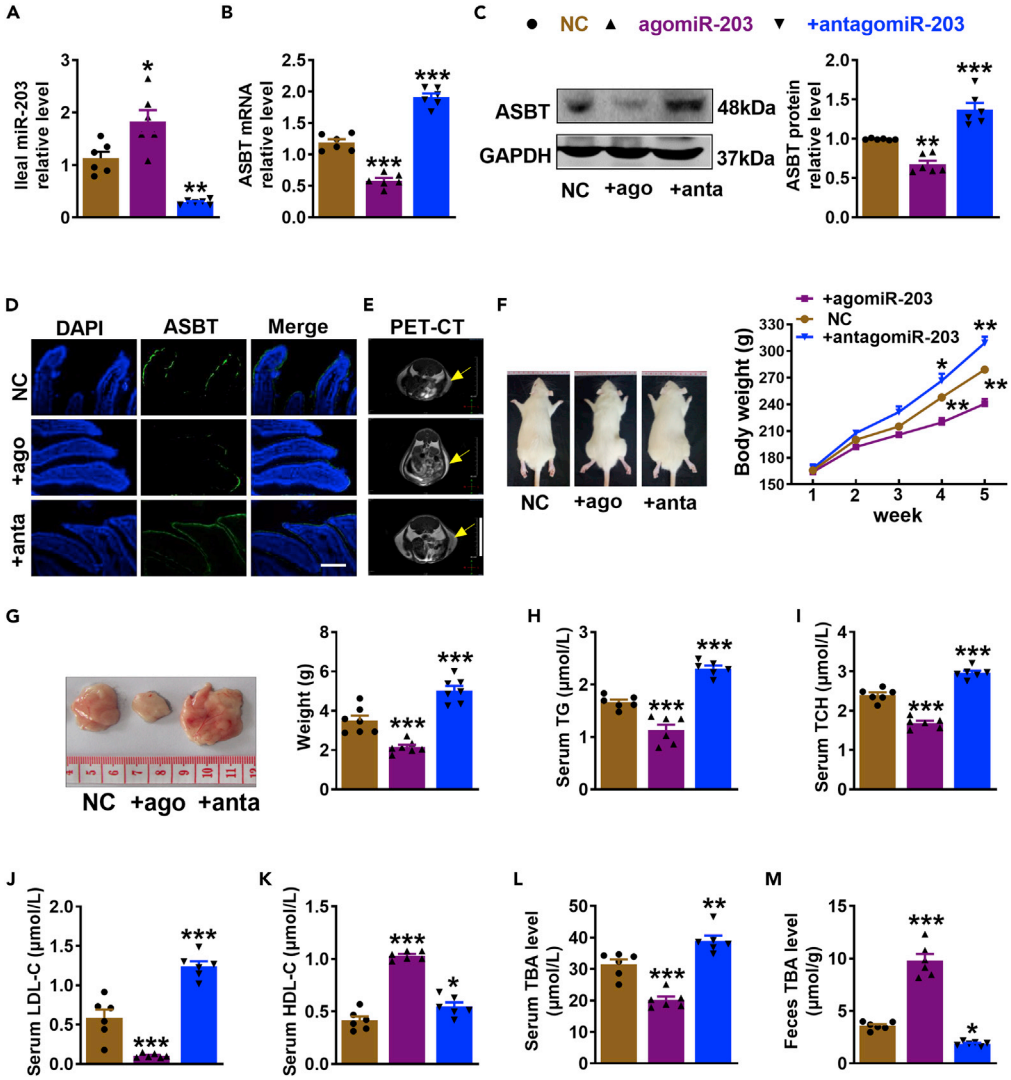

Figure 2. AgomiR-203 reduces body weight and improves lipid disorders in obese rats

Compared with rats intraperitoneally injected with mismatched nucleotides as a negative control (NC), rats were treated with agomiR-203 and antagomiR-203, respectively, to overexpress and silence miR-203.

(A) Overexpression and silencing efficiency of miR-203 in the terminal ileum of obese rats verification by qRT-PCR, n = 6.

(B and C) ASBT mRNA (B) and protein (C) levels in the terminal ileum of rats in different groups were detected by qRT-PCR and Western blot, n = 6.

(D) Immunofluorescence staining of ASBT protein (green) and nucleus (blue) in the brush border of ileum terminal of rats in different groups, Scale bar: 50 μm, n = 3.

(E) Fat distribution of rats in different groups was mapped by PET-CT, arrow points to the adipose tissue around ilium, Scale bar: 40 mm, n = 3.

(F) The weight changes of rats in different groups were monitored and recorded, n = 6.

(G) The changes in the periepididymal fat content of rats in different groups were observed and compared, n = 7.

(H–K) Serum lipid levels in rats. Serum (H) TG, (I) TCH, (J) LDL-C, and (K) HDL-C levels of rats in different groups were measured, n = 6.

(L and M) Serum (L) and fecal (M) total bile acid levels of rats in different groups were monitored, n = 6. The data are expressed as mean ± SEM, *p < 0.05, **p < 0.01, ***p < 0.001 vs NC by one-way ANOVA with Turkey's multiple comparison test.

SLC10A2 and the active promoter were constructed (Figure 3B). We found that the co-transfection of miR-203 mimic (miR-mimic) with the plasmid into HEK293 cells consistently produced less luciferase activity than the transfection of the plasmid alone (Control). Transfection of miR-203 inhibitor (miR-AMO) into the cells

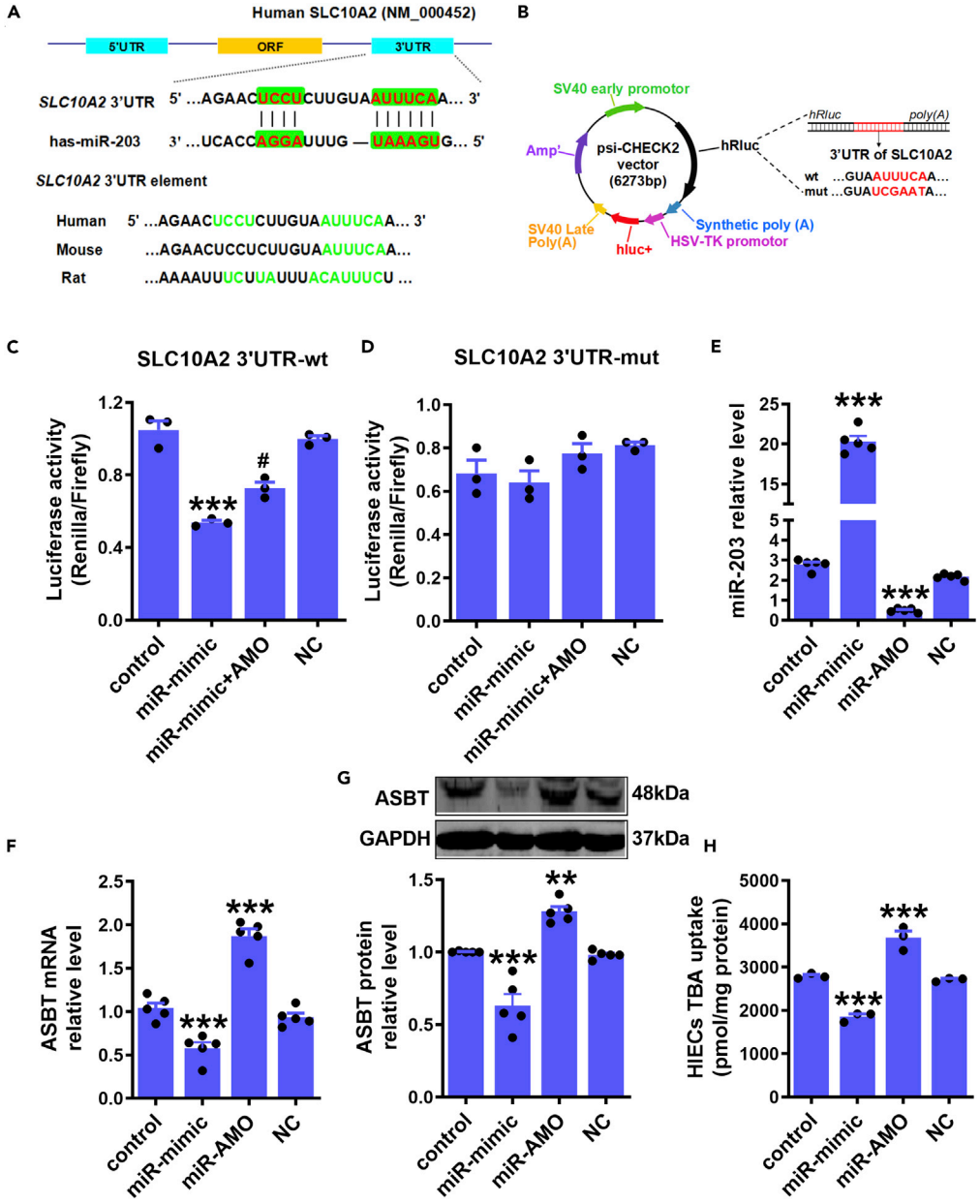

Figure 3. ASBT is a direct target of miR-203

(A) The complementary sequences between miR-203 and 3′UTRs of SLC10A2 were shown. And conserved sequences of SLC10A2 3′UTR element in humans, rats, and mice were marked in green font.

(B) Luciferase reporter containing the 3′UTR of SLC10A2 was constructed according to this schematic.

(C and D) Luciferase reporter assay was used to detect the inhibitory effect of miR-203 on (C) wild-type (wt) and (D) mutant (mut) 3′UTR of SLC10A2, n = 3.

(E) The expression level of miR-203 in HIECs after the transfection of miR-203 mimic (miR-mimic) and miR-203 inhibitor (miR-AMO) was detected by qRT-PCR, n = 5.

(F and G) The mRNA (F) and protein (G) expression levels of ASBT in HIECs in different groups were determined by qRT-PCR and Western blot, n = 5.

(H) TBA uptake by HIECs in different groups were detected, n = 3. The data are expressed as mean ± SEM, **p < 0.01, ***p < 0.001 vs control and #p < 0.05 vs miR-mimic by one-way ANOVA with Turkey's multiple comparison test.

diminished the inhibitory effect of miR-203. On the other hand, miR-203 couldn't suppress the translation of luciferase transcripts containing the mutant SLC10A2 3'UTR (Figures 3C and 3D). To further verify SLC10A2 as a cognate target gene for miR-203 for post-transcriptional repression, we determined the effects of miR-203 on the expression levels of the mRNA and protein products of this gene by qRT-PCR and Western blot analyses in human small intestine mucosal epithelial cells (HIECs) in culture. Transfection of miR-203 mimic significantly increased miR-203 levels within cells; whereas it decreased SLA10A2 expression, comparing to this, transfection of miR-203 inhibitor had reversed effect (Figures 3E–3G). To look into the possible impact of ASBT repression by miR-203 on BA uptake, we created a cellular model simulating enterohepatic circulation by adding BAs to the cell culture fluid. Total bile acid (TBA) uptake by HIECs was detected among groups. The results demonstrated that the cells with miR-203 mimic transfection had a diminished amount of TBA within cells compared to the control group. However, transfection of miR-203 AMO increased TBA uptake by HIECs (Figure 3H).

miR-203 transgenic mice are resistant to high-fat diet-induced obesity

Next, we generated miR-203 overexpression transgenic mice (TgN (miR-203)) and treated the mice with normal diet (ND) or HFD. qRT-PCR results confirmed the overexpression of miR-203 in different tissues of TgN (miR-203) mice (Figure S2). Body weight and fat deposition were measured. The results showed that TgN (miR-203) mice had significantly reduced body weight and fat deposition compared to WT mice with HFD treatment (WT-HFD). AntagomiR-203 administration increased the body weight and fat deposition of TgN (miR-203) mice to a comparative level with WT-HFD mice (Figures 4A–4C). Specifically, we found HFD induced a significant body weight increase in WT mice after 4 weeks (Figure 4D). Meanwhile, TgN (miR-203) mice exhibited a significant difference compared to WT-HFD mice after 4 weeks (Figure 4E). AntagomiR-203 treatment had marked effects compared to TgN (miR-203)-HFD group after 8 weeks (Figure 4E). The fat mass in the whole body of mice in different groups was tested using positron emission tomography-computed tomography (PET-CT) (Figures 4F and 4G). The results demonstrated that HFD induced a large amount of fat deposition in subcutaneous, abdomen, and pelvic cavity, as indicated by increased area and density of the gray zone. Expectedly, TgN (miR-203) mice had reduced fat deposition, while this effect was reversed by antagomiR-203 treatment. In addition, we also observed that TgN (miR-203) mice had smaller size of white adipose cells compared to WT mice under HDF condition and was reversed by antagomiR-203 treatment (Figure S3). Moreover, we didn't observe significant difference in body weight between WT-ND and TgN (miR-203)-ND groups.

miR-203 transgenic mice are resistant to high-fat diet-induced dyslipidemia

We then tested lipids levels in different groups of mice. Compared to WT-ND mice, WT-HFD mice had remarkably increased TCH levels in serum, liver, and feces, in contrast, these parameters were significantly decreased in TgN (miR-203) mice under HFD condition. Moreover, the antagomiR-203 treatment effectively reversed the beneficial effects of miR-203 overexpression on the amelioration of TCH levels (Figures 5A–5C). Serum TG levels were also detected. TgN (miR-203) mice had lower serum TG level compared to WT mice when fed HFD diet, which was diminished by antagomiR-203 treatment (Figure 5D). Intriguingly, we observed the color differences of feces among groups. Pale yellow color was shown in feces containing high lipids for example in WT-HFD mice, whereas deep yellow color was shown in WT-ND mice. Moreover, the feces color in TgN (miR-203)-HFD mice was even more pale than that of in WT-HFD mice, which indicated more lipid excretion in feces, and the phenomenon was eliminated after antagomiR-203 treatment (Figure 5E). Consistently, the ELISA results suggested that the fecal TG level was substantially increased in TgN (miR-203)-HFD mice compared to WT-HFD mice and decreased by antagomiR-203 treatment (Figure 5F). Moreover, TgN (miR-203)-HFD mice had remarkably decreased serum LDL level (Figure 5G), and increased HDL level when compared with WT-HFD mice (Figure 5H), whereas antagomiR-203 treatment significantly deteriorated dyslipidemia in (miR-203)-HFD mice. To further determine the impact of overexpression of miR-203 on the clearance of dietary fats (chylomicrons) in the peripheral circulation, olive oil was administered to mice by gastric gavage and plasma TAGs (triacylglycerols) and NEFAs (non-esterified free fatty acids) levels were detected at different time points. We found that postprandial plasma levels of TAGs and NEFAs were remarkably reduced in TgN (miR-203)-HFD mice as compared to WT obese mice, which was reversed by antagomiR-203 treatment (Figures 5I and 5J).

miR-203 transgenic mice had elevated fecal bile acid excretion

TBA pools in different groups of mice were then evaluated. Elevated serum TBA and decreased fecal TBA levels were observed in obese mice. Overall, TgN (miR-203) mice showed increased TBA excretion in feces,

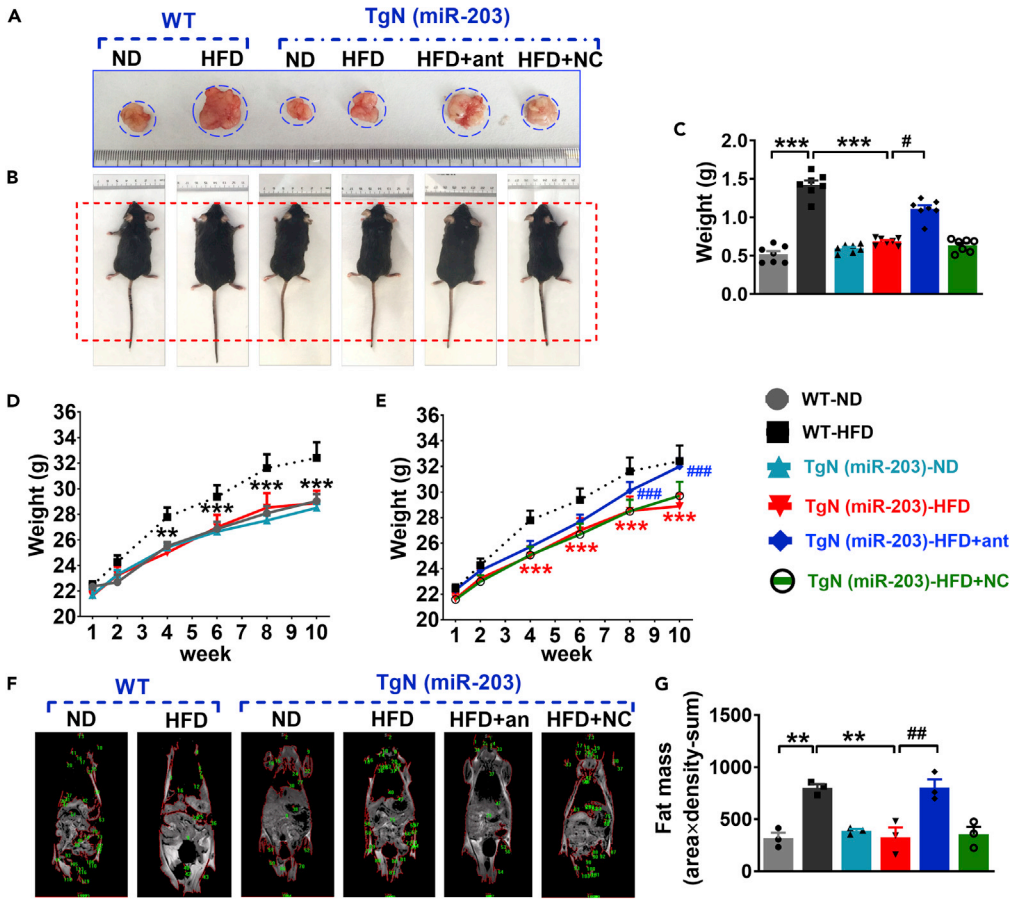

Figure 4. TgN (miR-203) mice are resistant to HFD-induced obesity

(A and C) Both WT and TgN (miR-203) mice were treated with HFD to induce obesity, and mice were treated with or without antagomiR-203 and NC. The changes in the fat content of mice in different groups were observed (A) and weighed (C), n = 7.

(B, D, and E) The body weight of mice in different groups was observed (B) and recorded (D and E), n = 7.

(F and G) Fat distribution of mice in different groups was mapped by PET-CT and compared, n = 3, the green marks represent borders of calculated fat. The data are expressed as mean ± SEM, **p < 0.01, ***p < 0.001 vs WT-HFD, #p < 0.05, ##p < 0.01 vs TgN (miR-203)-HFD, by one-way ANOVA with Turkey's Multiple Comparison Test.

decreased liver TBA level, and no significantly altered serum TBA level simultaneously, relative to their WT counterparts (Figures 6A–6C). These results suggested the unique characteristics of TBA pool in TgN (miR-203) mice, which were similar to that of ASBT knockout mice (Rao et al., 2016). When comparing TgN (miR-203) mice to WT mice under HFD condition, TgN (miR-203) mice had more excretion of TBA in feces, whereas was inhibited by antagomiR-203 treatment (Figures 6A–6C).

In addition, the alterations of the serum BA profile caused by miR-203 overexpression were further detected. The results showed that miR-203 overexpression significantly altered serum BA composition under HFD condition, by reducing concentrations of primary BAs tauro-β-muricholic acid (TβMCA) (Figure S4A), taurocholic acid (TCA) (Figure S4B) and taurochenodeoxycholic acid (TCDCA) (Figure S4C), and increasing UDCA (ursodeoxycholic acid) (Figure S4D). For secondary bile acid, miR-203 overexpression remarkably decreased TωMCA (tauro-ω-muricholic); but increased TUDCA (tauroursodeoxycholic acid), TDCA (tauro-deoxycholic acid), and DCA (deoxycholic acid) (Figures S4E–S4H). Studies have revealed that TβMCA (Oteng et al., 2021), TCA (Azzimato et al., 2021), TCDCA (Zhang et al., 2021a), and TωMCA (Nie et al., 2012)were significantly increased in obesity; while the downregulated UDCA (Dong et al., 2021), TUDCA (Zhang et al., 2021b), TDCA (Lei et al., 2017) and DCA (Yoshimoto et al., 2013) were harmful to liver or lipid metabolism. These parameters were corrected in miR-203 overexpression mice. We then examined the expression of important genes related to BA metabolism in liver. CYP7A1 is the rate-limiting enzyme for

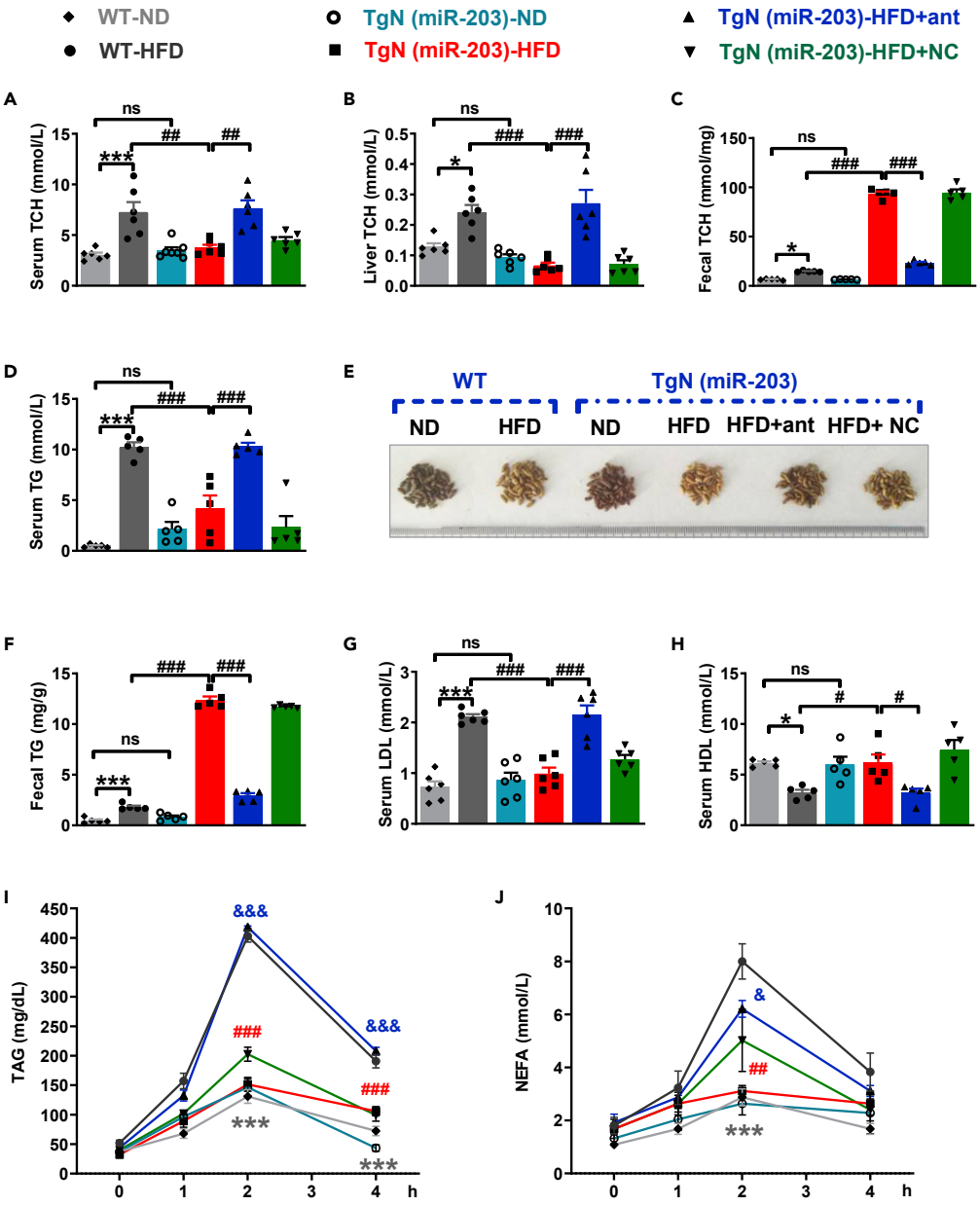

Figure 5. TgN (miR-203) mice are resistant to HFD-induced dyslipidemia

(A–C) (A) Serum TCH, n = 5 (B) liver TCH, n = 6, and (C) fecal TCH levels of mice in different groups were measured, n = 5.

(D) Serum TG levels of mice were measured, n = 5.

(E) The color of feces of different groups of mice was observed.

(F) Fecal TG levels of mice in different groups were measured, n = 5.

(G and H) Serum LDL-C n = 6 and (H) HDL-C levels were measured, n = 5.

(I and J) Oral lipid tolerance test showing the clearance of (I) TAG and (J) NEFA from the plasma of different groups of mice fasted for 4 h followed by oral gavage of olive oil, n = 3. The data are expressed as mean ± SEM, *p < 0.05, ***p < 0.001 vs WT-HFD, #p < 0.05, ##p < 0.01, ###p < 0.001 vs TgN (miR-203)-HFD, &p < 0.05, &&&p < 0.001 vs TgN (miR-203)-HFD, by one-way ANOVA with Turkey's Multiple Comparison Test.

BA synthesis in liver. Consistent with the previous study, we also found the upregulation of CYP7A1 in obese mice that is caused by increasing in BA synthesis under HFD condition (Jiao et al., 2018) (Pozzo et al., 2016) (Muraoka et al., 2011). TgN (miR-203) mice expressed increased CYP7A1 expression levels, which was possibly owing to the feedback effects induced by decreased serum BA pool after ASBT

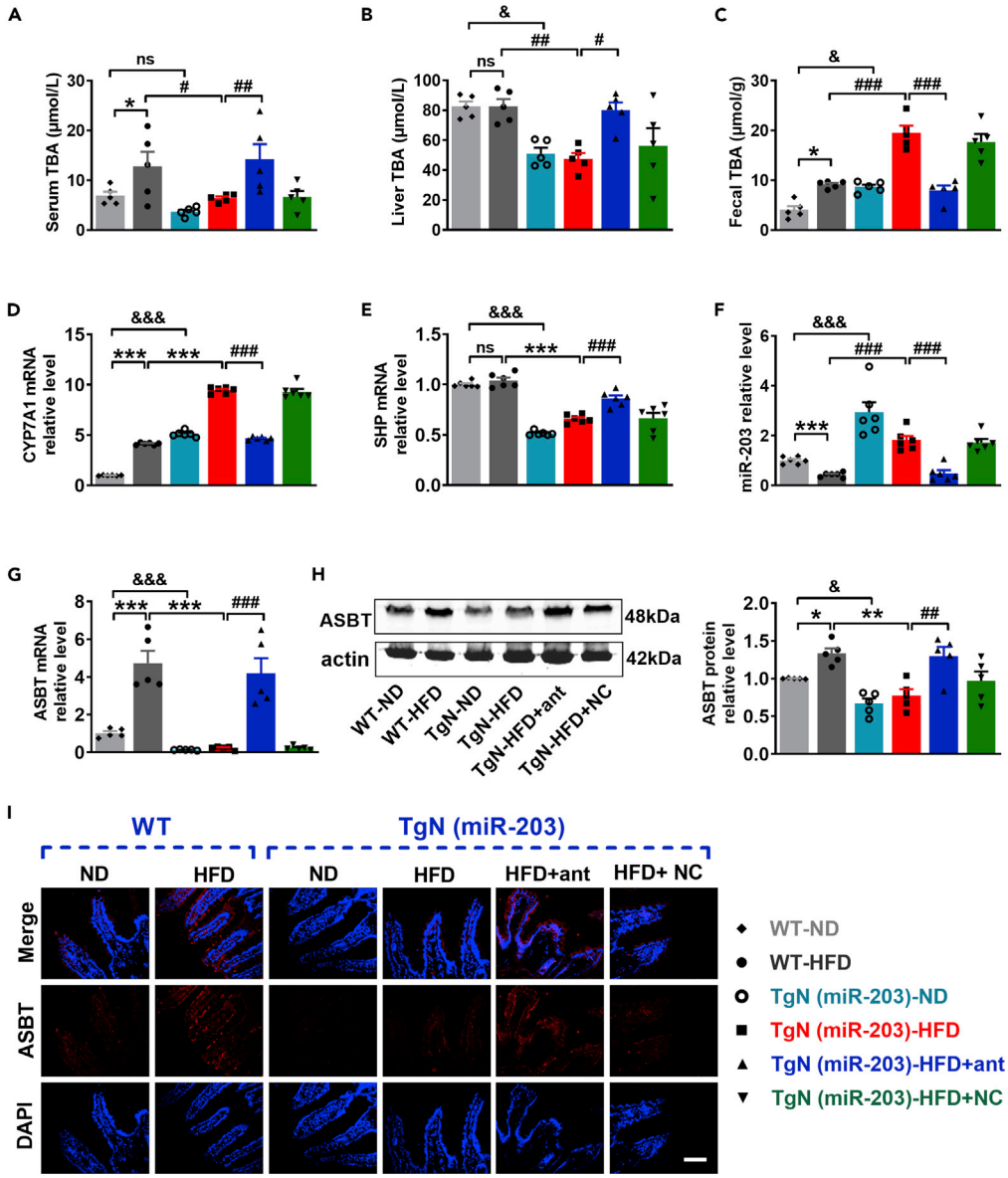

Figure 6. miR-203 overexpression alters BA content in obese mice

(A–C) TBA levels of (A) serum, (B) liver, and (C) feces were detected, n = 5.

(D and E) The mRNA expression levels of (D) CYP7A1 and (E) SHP in the liver of mice in different groups were analyzed by qRT-PCR, n = 6.

(F) The expression level of miR-203 in cecum tissue of mice in different groups was determined by qRT-PCR, n = 6.

(G and H) The (G) mRNA and (H) protein expression levels of ASBT in cecum tissue of mice in different groups were analyzed by qRT-PCR and Western blot, n = 5.

(I) Immunofluorescence staining of ASBT protein in brush border of terminal ileum of rats in different groups, Scale bar: 50 μm, n = 3. The data are expressed as mean ± SEM, *p < 0.05, **p < 0.01, ***p < 0.001 vs WT-HFD, #p < 0.05, ##p < 0.01, ###p < 0.001 vs TgN (miR-203)-HFD, &p < 0.05, &&&p < 0.001 vs WT-ND, by one-way ANOVA with Turkey's multiple comparison test.

knockdown. However, antagomiR-203 treatment diminished the upregulation of CYP7A1 in TgN (miR-203) mice (Figure 6D). SHP was the transcriptional regulator of CYP7A1, which was not altered in obese mice but had an opposite expression profile in TgN (miR-203) mice to CYP7A1, as indicated by downregulation in both ND and HFD treated miR-203 transgenic mice. AntagomiR-203 treatment also reversed this effect in transgenic mice (Figure 6E).

Furthermore, miR-203 and ASBT expression levels were validated from the cecum of mice in different groups. The level of miR-203 was markedly decreased in WT-HFD mice and increased in TgN (miR-203) mice compared to WT-ND mice. AntagomiR-203 treatment decreased the miR-203 level in TgN (miR-203)-HFD mice (Figure 6F). qRT-PCR and Western blot results demonstrated that compared to WT-ND mice, ASBT mRNA and protein levels were increased in WT-HFD mice. TgN (miR-203) mice had decreased expression levels of ASBT, which was reversed by antagomiR-203 treatment (Figures 6G–6I).

TCF7L2 is the upstream activator of miR-203

Why the downregulation of miR-203 in obese rats should be inquired. Gene TCF7L2 is expressed as a protein called TCF-4, which was involved in the Wnt signaling pathway and played an important role in diabetes and obesity development (Duncan et al., 2019; Nanfa et al., 2015). We forecasted that it may be an important positive transcription factor of miR-203 by using the ChIPBase database (Figure S5). The expression of TCF7L2 was first compared in lean and obese rats. The results suggested a significant decrease in the TCF7L2 protein level in the ileum of obese rats (Figure 7A). We then transfected TCF7L2 overexpression plasmid into HIECs, as a consequence, the miR-203 level was remarkably increased by TCF7L2 overexpression (Figures 7B and 7C). Next, we identified putative TCF7L2 recognition sites within the 2000 bp region upstream to pre-miR-203. We set out to evaluate the role of the TCF7L2 in regulating the transcription of the miR-203 gene. To this end, a fragment that contains the perfect binding sites between TCF7L2 and miR-203 promoter were constructed as a decoy oligodeoxynucleotide (dODN). As expected, transfection of dODN competitively decoyed the TCF7L2-miR-203 complex, which led to the inhibition of miR-203 expression (Figure 7D). We also conducted a luciferase reporter vector that inserted the miR-203 promoter. Co-transfection of the vector with the decoy oligodeoxynucleotide (dODN) into HIEC cells caused a substantial reduction in luciferase activities (Figure 7E). To verify the physical interaction between TCF7L2 and the *cis*-acting elements of miR-203, we also carried out EMSA (electrophoretic mobility shift assay) in conjunction with super-shift to assess the ability of TCF7L2 to bind the putative *cis*-acting elements of the miR-203 host genes. We incubated each probe, a synthesized, digoxigenin-labeled (DIG-labeled) putative TCF7L2 *cis*-acting element, with nuclear extract from HIECs. As depicted in Figure 7F, a shifted band representing protein-DNA binding was identified, which was eliminated upon the addition of excessive competitive probes, but was supershifted by the antibody to TCF7L2. We then subsequently conducted ChIP assay to further verify the protein-DNA interactions that occur inside the nucleus of living cells. The results also confirmed the binding of TCF7L2 to the *cis*-acting element of the miR-203 (Figure 7G).

Blood miR-203 level could indicate obesity in population

To see whether our experimental data have any clinical implications, we measured plasma and ileal miR-203 levels, as well as ileal ASBT level in individuals with different BMI. Correlograms revealed that miR-203 was inversely correlated with BMI in a comparable strong correlation, no matter in plasma ($R = -0.68$, $p = 2.4e-15$) (Figure 8A) and ileum ($R = -0.74$, $p = 1.3e-11$) (Figure 8C). The decrease in the miR-203 level was significant even when BMI was over 24 (Figures 8B and 8D). Moreover, as the BMI increases, the expression of ASBT in ileum was upregulated in mRNA levels ($R = 0.54$, $p = 1e-05$) (Figure 8E); and was significant in populations with BMI over 28 (Figure 8F). The above results revealed that miR-203 and ASBT expression might be therapeutic biomarkers for obesity-prone; in the meanwhile, miR-203 was more sensitive to indicating obesity than ASBT.

DISCUSSION

Collectively, our study presents several new findings pertinent to obesity. First, miR-203 was downregulated and ASBT was upregulated in rat and mice models of obesity as well as human subjects with overweight and obesity. Second, ASBT was validated as a cognate target for miR-203 which explains the reciprocal relationship between miR-203 and ASBT expression. TCF7L2 acted as an upstream activator of miR-203. Third, agomiR-203 treated rats or miR-203 overexpression transgenic mice were resistant to HFD-induced obesity and dyslipidemia through increasing TBA and lipids excretion, whereas the knockdown of endogenous miR-203 alone by antagomiR-203 was sufficient to create the above metabolic disorders in otherwise healthy rats. These findings indicate that the HFD downregulated miR-203 that in turn upregulated ASBT as a result of derepression or removal of tonic repression, leading to enhanced enterohepatic circulation thereby hyperlipidemia and obesity. In other words, miR-203 is an anti-obesity miRNA that controls obesity and hyperlipidemia by repressing SLC10A2 (the gene encoding ASBT) expression, blocking the enterohepatic circulation, and increasing BA excretion, enabling exogenous fats excretion.

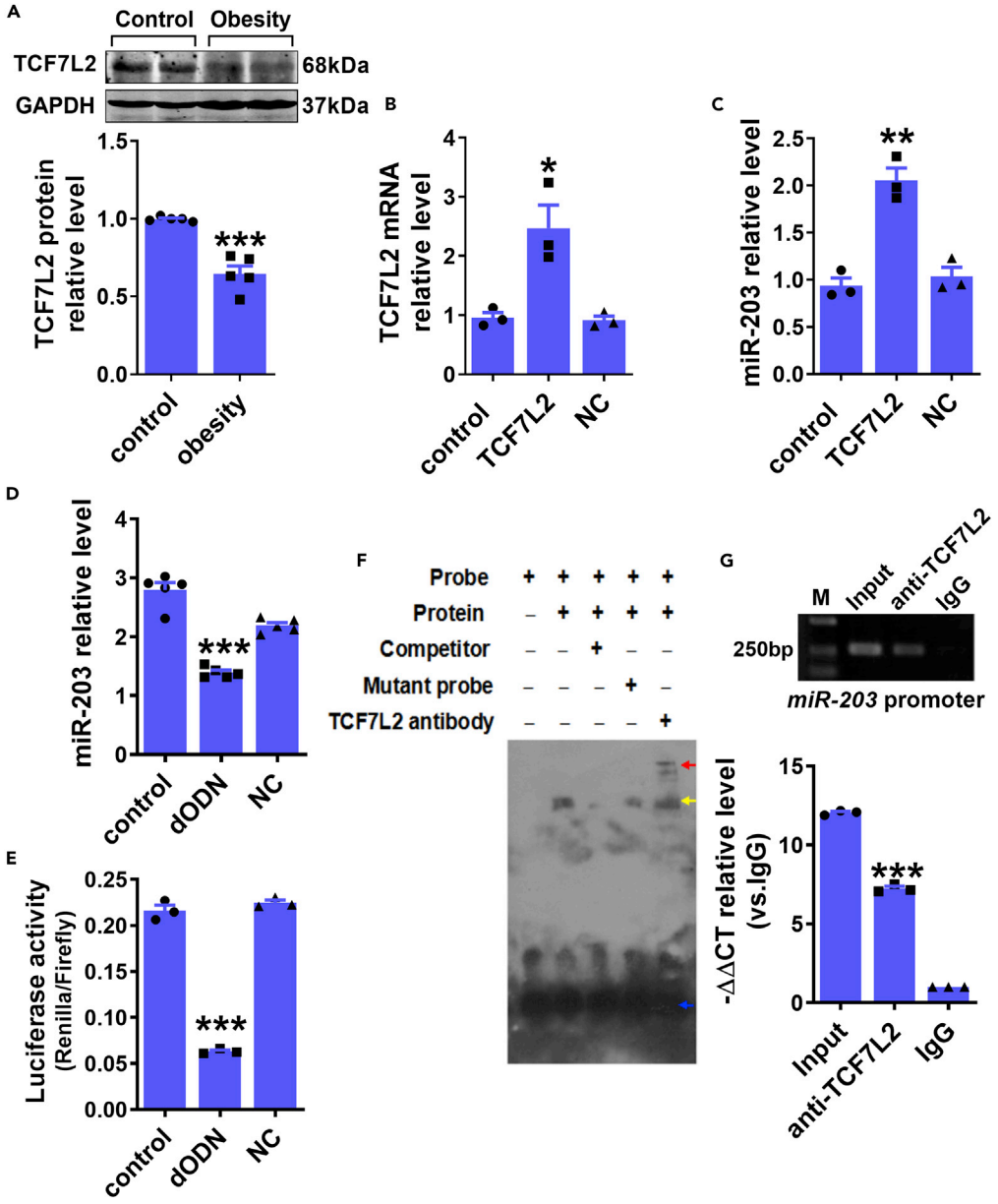

Figure 7. TCF7L2 is a transcriptional factor of miR-203

(A) The protein expression level of TCF7L2 in the ileum of control and obese rats was analyzed by Western blot, n = 5.

(B and C) HIECs were transfected with TCF7L2 overexpression plasmid. The levels of (B) TCF7L2 mRNA and (C) miR-203 in HIECs in different groups were determined by qRT-PCR, n = 3.

(D and E) HIECs were transfected dODN. The levels of (D) miR-203, n = 5 and (E) luciferase activities in HIECs in different groups were detected, n = 3.

(F) EMSA to test *in vitro* binding of TCF7L2 to the promoter region of human host genes for miR-203. Note shifted band representing protein-DNA binding (yellow arrow), abolished with the excess nonlabeled probe. Supershifted band (red arrow) represents TCF7L2-miR-203 binding in presence of the anti-TCF7L2 antibody.

(G) ChIP assay to test the binding of TCF7L2 to the human host gene of miR-203. Top: PCR products of TCF7L2-miR-203 binding sites following immunoprecipitation with anti- TCF7L2 antibody. Bottom: host gene binding measured by qPCR following ChIP, expressed as fold-changes over IgG-negative control. Input: genomic DNA without immunoprecipitation, n = 3. The data are expressed as mean ± SEM, *p < 0.05, **p < 0.01, ***p < 0.001 vs control in (A-E), vs Input in (G) by one-way ANOVA with Turkey's multiple comparison test.

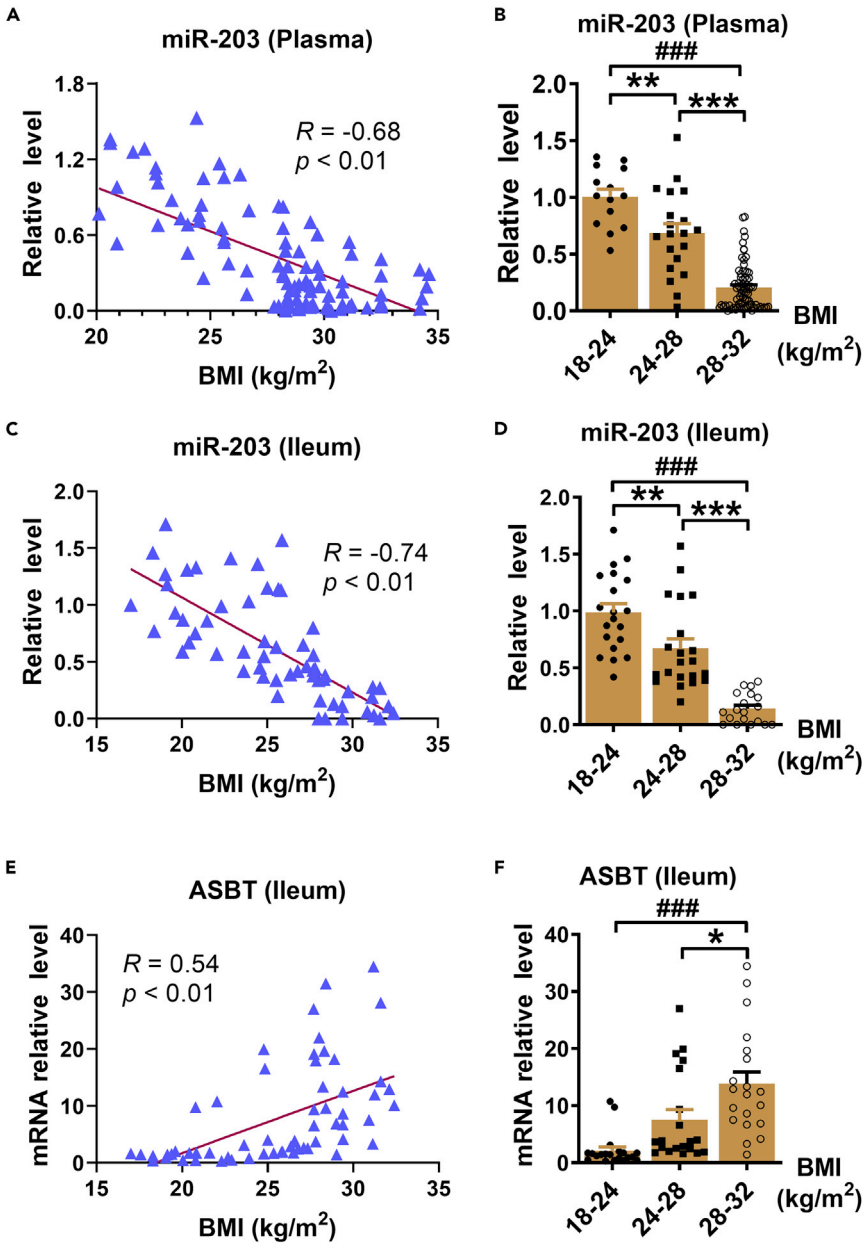

Figure 8. Correlation between miR-203 or ASBT expression levels with obesity

(A–D) The expression level of miR-203 in human plasma (A and B) and ileum (C and D) of individuals with different BMI were determined by qRT-PCR, 105 samples in A and B, 60 samples in C and D.

(E and F) The expression level of ASBT mRNA in the human ileum of individuals with different BMI was determined by qRT-PCR, 60 samples in (E and F). R value is analyzed by personal correlation of SPSS. The data are expressed as mean ± SEM, *p < 0.05, **p < 0.01, ***p < 0.001 vs BMI (24–28 kg/m^2), ###p < 0.001 vs BMI (18–24 kg/m^2) by one-way ANOVA with Turkey's multiple comparison test.

MiRNAs are comparatively stable within the body than other RNA molecules. The half-life of miRNAs (approximately 28 h to 5 days) is estimated to be 10 times longer than that of mRNA molecules, which made it possible to be a therapeutic target (Kwekkeboom et al., 2014). AgomiR-203 and antagomiR-203 used in our research were efficient without regard to serious tissue specificity and side effects. However, there is still a persistent need for approaches to exert better efficacy via increasing tissue-specific uptake and preventing off-target effects of miRNA. In our study, we found miR-203 was a changeable molecule in the plasma of population with different BMI and might be as a predictable plasma marker for obesity

generation in advance. Several studies have demonstrated that differences in plasma miR-203 expression could indicate or predict disease development such as colorectal cancer, cervical cancer, and rheumatoid arthritis (Filková et al., 2014; Hasanzadeh et al., 2019; Hur et al., 2017). However, it is not fully explained what is the source of miR-203? And how are they released into circulation? Future studies are necessary to unravel these mechanisms.

The functions of miR-203 in cancers and neurodegenerative diseases had been profoundly revealed by published studies. Swarup and colleagues suggested that overexpression of miR-203 could influence related co-expression patterns of mRNA and induce neuronal cell death, which participated in the regulation of neurodegeneration diseases (Swarup et al., 2019). In addition, miR-203 is commonly recognized as a tumor suppressor by inhibiting tumor proliferation and metastasis. For example, Jimenez and colleagues proved that the activation of the FGFR1/ERK1/2 signaling pathway promotes the expression of ZEB1 that regulates ADAMDEC1 expression through targeting miR-203, establishing a positive feedback loop in glioblastomas (Jimenez-Pascual et al., 2019). In breast cancer, miR-203 was downregulated in the breast epithelium of women with a high mammographic density that repressed matrix stiffness (Northey et al., 2020). Besides, overexpression of miR-203 inhibits proliferation and metastasis but induces apoptosis of CSCC cell line SCL-1 (Ting et al., 2020). Recently, some studies also revealed the beneficial effects of miR-203 in metabolic-related disorders. Brandão and colleagues suggested that exercise training-induced DICER-miR-203-3p upregulation in adipocytes were a key adaptive response that coordinated signals from working muscle to promote whole-body metabolic adaptations (Brandão et al., 2020). Jin and colleagues suggested miR-203 was downregulated in the diabetic heart and exhibited anti-fibrosis when they were overexpressed (Jin, 2021). In addition, few studies suggested the promotion effects of miR-203 on adipose tissue metabolism under HFD condition. Guo and colleagues proved that miR-203 promoted white adipose tissue browning in cold exposed mice and improved glucose tolerance in HFD-fed mice by repressing interferon-γ (Guo et al., 2019). Our results also proved the beneficial role of miR-203 in obesity. Of note, our study was the first to reveal the functional effects of miR-203 on the amelioration of obesity and dyslipidemia through regulating BAs homeostasis, based on experiments in transgenic mice, obese rat model, and target cells. Our experimental results showed that the administration of agomiR-203 to obese rats for 4 weeks could significantly reduce the weight of obese rats by 14%. Moreover, TgN (miR-203) mice received HFD for 9 weeks and lost 11% of body weight compared with WT mice, which indicated the superior weight loss effect of miR-203 overexpression. On the other side, exogenous administration of antagomiR-203 reversed the weight-loss effect of miR-203. Decreased accumulation of white adipose tissue in subcutaneous, abdominal, and pelvic cavities is in accord with the weight-loss effect of miR-203 as shown by magnetic resonance imaging (MRI) results. However, the increased excretion of TGs and cholesterols from feces in TgN (miR-203) mice contributes to the reduction of white adipose tissue accumulation, weight loss, and amelioration of dyslipidemia.

Bile acids (BAs) are synthesized from cholesterol in the liver and are necessary for lipid absorption (Trampert et al., 2021). Primary BAs are produced in the liver and then secreted to the intestinal lumen in the form of conjugates. The conjugated primary BAs are further transformed into secondary BAs via deconjugation and multistep dehydroxylation reactions conducted by gut bacteria (Perino et al., 2021). Normally, reabsorption of BA in the terminal ileum through enterohepatic circulation leads to the accumulation of a certain mass of BA within the body, commonly referred to as the BA pool. BA pool is existed in blood, liver, and intestine, in which the composition and amount of BAs are co-regulated by specific metabolizing enzymes and transporters (Fiorucci et al., 2021). An average of 2g of BAs cycles 12 times per day in humans and only 5% of the total BAs escape reabsorption and eliminate into the feces. Importantly, BA synthesis and excretion are determinants for maintaining lipids metabolism (Kunst et al., 2021). Increasing fecal BA excretion leads to the consumption of cholesterol for BA synthesis and the reduction of lipid absorption. Dysregulation of BA synthesis and metabolism is also related to metabolic disorders including obesity, diabetes, and chronic liver diseases (Ding et al., 2021). Consistent with the current study, in the obese rats, we also found a remarkable increase of BA pool in the circulation of obese rats, whist a decrease in BA excretion from feces. However, in HFD rats treated with agomiR-203 or in the TgN (miR-203) mice fed with HFD, the circulation and liver BA pool were diminished owing to more BAs excretion. All these results further confirmed that the optimal shrink of the circulatory BA pool was effective for ameliorating obesity and dyslipidemia. The consistent results were also exerted by BAs chelators such as chitosan (Jang et al., 2017), neurotensin (Gui and Carraway, 2001), and sevelamer (Brønden et al., 2018). Importantly, although the exhilarating outcomes of BAs chelator for the treatment of obesity and dyslipidemia, the abnormities in

gastrointestinal tract such as persistent diarrhea was nonnegligible. Response to this point, we did observe the imperceptible gastrointestinal side effects in miR-203 overexpression mice, as indicated by the normal form of feces in different groups of TgN (miR-203) mice. Moreover, we observed a unique phenotype of BA pool in TgN (miR-203) mice, as shown by decreased liver BA content and increased BA excretion. The downregualtion of ASBT expression might contribute to the conversion of the phenotype, which was also described for ASBT knock-out mice (Rao et al., 2016). Meanwhile, the smaller size of the BA pool stimulated the upregulation of CYP7A1 and downregulation of SHP for BA synthesis in the liver of Tg (miR-203) mice. However, the non-substantial change in the BA pool in Tg (miR-203) mice didn't influence the lipids profile and body weight of the mice.

Moreover, we found that miR-203 overexpression altered the BA profile in mice. Cholate (CA) and chenodeoxycholate (CDCA) are primary BAs that are synthesized in the liver from cholesterol and subsequently conjugated with taurine or glycine to form bile salts for the preparation of secretion into bile canaliculi. In the intestine, primary BAs will be catalyzed into secondary BAs through 7α-dehydroxylation or epimerization reactions, notably, CA to deoxycholic acid (DCA), CDCA to ursodeoxycholic acid (UDCA), and lithocholic acid (LCA). Besides, muricholic acids including α-MCA and β-MCA are transformed into ωMCA, hyodeoxycholic acid (HDCA), and so forth (Hofer, 2021). The functions and molecular mechanisms of different BAs in diseases are diverse and complex. We found some BAs were markedly regulated by miR-203 as shown in Figure S4. The primary BAs including TβMCA (Oteng et al., 2021), TCA (Azzimato et al., 2021) and TCDCA (Zhang et al., 2021a) and TωMCA (Nie et al., 2012) were increased in obese mice, the phenomenon was also shown in other studies, as these BAs were considered toxic for hepatic cells owing to the increase of oxidative stress and cell apoptosis. UDCA is extensively used for the treatment of many hepatobiliary diseases such as cholestatic liver diseases and non-alcoholic steatohepatitis because of its positive effects on steatosis and inflammation (Dong et al., 2021). Studies have revealed that taurine-conjugated UDCA could increase insulin sensitivity in muscle, liver, and white adipose tissue of obese humans and mice (Schattenberg et al., 2021). Besides, UDCA could increase the synthesis and utilization of cholesterol in liver and subsequently ameliorate dyslipidemia through the inactivation of farnesoid X receptor (Kübeck et al., 2016). Our study further confirmed the decrease of UDCA and TUDCA in obese condition. TDCA was also found the downregulation in obesity in other published studies (Lin et al., 2019), and restored TDCA levels imitate the effects of bariatric surgery (Quante et al., 2021). Besides, DCA was shown beneficial for metabolic disorders. Elevated levels of DCA were observed in obesity and it could activate the adipose G-protein-coupled bile acid receptor, GPBAR1. This activation increased the expression of UCP1 and mitochondrial creatine kinase CKMT2, leading to the increased thermogenesis of white adipose tissue (Wu et al., 2021). Overall, we found that miR-203 converted the circulatory BA profile into a beneficial type. The inhibitory effects of miR-203 on ASBT might contribute to the BA profile diversity, whereas the selectivity for BA uptake caused by miR-203 still needs further clarification.

ASBT is considered an attractive target for the intervention of diseases related to BA, cholesterol, lipid, glucose, and so forth. Several studies have also reported an increase in the ASBT level in obesity (Sundaram et al., 2019; van de Peppel et al., 2020). However, the upstream regulators that contribute to ASBT upregulation were nearly discovered. Our study firstly identified that miR-203 acted as a trigger for ASBT upregulation in obesity and set it as a genetic tool for weight loss and reducing blood lipids by inhibiting ASBT expression, which provides a new anti-ASBT therapy distinct from current chemical therapies. Elobixibat as an ASBT inhibitor was recently launched in Japan for the treatment of CIC (Bassotti et al., 2021). Linerixibat was a potent and non-absorbable ASBT inhibitor for the treatment of T2D, but was suspended from the development program after the phase II trial (Zamek-Gliszczynski et al., 2021). Despite the successes of ASBT targeting drugs that have been proved in preclinical and clinical studies, less such prodrugs have progressed to market. Moreover, recent studies revealed that ASBT knock-out might exert better protective effects against metabolic disorders compared to ASBT inhibitor (Rao et al., 2016). More significant advances and extensive research efforts need to be made to further study ASBT, BA, and the transport mechanism.

miRNA expression is regulated by many factors, including long non-coding RNA, transcription factors, epigenetic modifications, and so forth. Liu and other studies have found that lncRNA SNHG14 promotes renal cancer metastasis and invasion by inhibiting miR-203 expression (Liu et al., 2017); Marthaler and colleagues reported CEBPα as a transcription factor of miR-203, which could promote the expression of miR-203 in human keratinocytes (Marthaler et al., 2017). We explored the upstream regulator of miR-203 by

predicting its transcription factors in the ChIPBase database. Among them, TCF7L2 has been proved as a susceptibility gene for obesity and diabetes (Mansour Aly et al., 2021); however, its molecular mechanism in obesity is not totally clear. Important expression similarities were identified between TCF7L2 and miR-203 in our study. The transcriptional activation on miR-203 by TCF7L2 was also confirmed, which provides a possible mechanism for the anti-obesity effect of TCF7L2.

In summary, this study clarifies the important role of the TCF7L2/miR-203/ASBT axis in obesity, confirming the significant weight-loss and lipid-lowering effects of miR-203 overexpression, which provides a new therapeutic approach for early warning, prevention, and treatment of obesity.

Limitations of the study

The anti-obesity effect of miR-203 was proved in mice. The comparable effects remain to be assessed in human studies, although we have evaluated the prognostic potential of miR-203 in human plasma. In view of the utilization of small RNA molecules in the clinic, the translation research is anticipated and valuable. We also note that the genetic tools used in our animal studies for miR-203 knockdown are antagomiR-203. Experiments in cecum-specific miR-203 KO mice would be better for further performance. Finally, it is possible that there are additional relevant mRNA targets of miR-203, and this should be the subject of future studies.

STAR★METHODS

Detailed methods are provided in the online version of this paper and include the following:

- KEY RESOURCES TABLE
- RESOURCE AVAILABILITY
  - Lead contact
  - Materials availability
  - Data and code availability
- EXPERIMENTAL MODEL AND SUBJECT DETAILS
  - Study approval
  - Obese rat model
  - MiR-203 overexpression transgenic mice
  - HIEC cell line
  - Human samples
- METHOD DETAILS
  - Measurement of serum lipid and total bile acid
  - Measurement of serum bile acid profile
  - Fat tolerance test
  - RNA extraction and quantitative real-time PCR
  - Western blot
  - Immunofluorescence
  - Luciferase reporter assay
  - dODNs synthesis
  - Cell transfection
  - ChIP assay
  - EMSA
- QUANTIFICATION AND STATISTICAL ANALYSIS

SUPPLEMENTAL INFORMATION

Supplemental information can be found online at https://doi.org/10.1016/j.isci.2022.104708.

ACKNOWLEDGMENTS

This study was funded by the National Natural Science Foundation of China (91949130, 81961138018, 81903610, 81730012) and HMU Marshal Initiative Funding (HMUMIF-21022).

AUTHOR CONTRIBUTIONS

Y.Z. and B.Y. designed the studies, and X.L. and F.C. performed most of the experiments. X.B., L.Z., T.Z., L.W., P.T., and L.J. performed experiments on transgenic mice. M.L., X.W., X.C., and M.W. assisted with cell culture, Western blot, and ELISA experiments. C.Y. and F.P. collected clinical samples. X.G. and N.M. generated transgenic mice. X.L. analyzed the data and wrote the article.

DECLARATION OF INTERESTS

The authors declare no competing interests.

Received: January 18, 2022
Revised: May 29, 2022
Accepted: June 28, 2022
Published: August 19, 2022

REFERENCES

Azzimato, V., Chen, P., Barreby, E., Morgantini, C., Levi, L., Vankova, A., Jager, J., Sulen, A., Diotallevi, M., Shen, J.X., et al. (2021). Hepatic miR-144 drives fumarase activity preventing NRF2 activation during obesity. Gastroenterology *161*, 1982–1997.e11. https://doi.org/10.1053/j.gastro.2021.08.030.

Bassotti, G., Usai Satta, P., and Bellini, M. (2021). Chronic idiopathic constipation in adults: a review on current guidelines and emerging treatment options. Clin. Exp. Gastroenterol. *14*, 413–428. https://doi.org/10.2147/ceg.s256364.

Brandão, B.B., Madsen, S., Rabiee, A., Oliverio, M., Ruiz, G.P., Ferrucci, D.L., Branquinho, J.L., Razolli, D., Pinto, S., Nielsen, T.S., et al. (2020). Dynamic changes in DICER levels in adipose tissue control metabolic adaptations to exercise. Proc. Natl. Acad. Sci. USA *117*, 23932–23941. https://doi.org/10.1073/pnas.2011243117.

Brønden, A., Mikkelsen, K., Sonne, D.P., Hansen, M., Våben, C., Gabe, M.N., Rosenkilde, M., Tremaroli, V., Wu, H., Bäckhed, F., et al. (2018). Glucose-lowering effects and mechanisms of the bile acid-sequestering resin sevelamer. Diabetes Obes. Metab. *20*, 1623–1631. https://doi.org/10.1111/dom.13272.

Castellanos-Jankiewicz, A., Guzmán-Quevedo, O., Fénelon, V.S., Zizzari, P., Quarta, C., Bellocchio, L., Tailleux, A., Charton, J., Fernandois, D., Henricsson, M., et al. (2021). Hypothalamic bile acid-TGR5 signaling protects from obesity. Cell Metab. *33*, 1483–1492.e10. https://doi.org/10.1016/j.cmet.2021.04.009.

Ding, L., Yang, Q., Zhang, E., Wang, Y., Sun, S., Yang, Y., Tian, T., Ju, Z., Jiang, L., Wang, X., et al. (2021). Notoginsenoside Ft1 acts as a TGR5 agonist but FXR antagonist to alleviate high fat diet-induced obesity and insulin resistance in mice. Acta Pharm. Sin. B *11*, 1541–1554. https://doi.org/10.1016/j.apsb.2021.03.038.

Dong, X., Luo, Y., Lu, S., Ma, H., Zhang, W., Zhu, Y., Sun, G., and Sun, X. (2021). Ursodesoxycholic acid alleviates liver fibrosis via proregeneration by activation of the ID1-WNT2/HGF signaling pathway. Clin. Transl. Med. *11*, e296. https://doi.org/10.1002/ctm2.296.

Duncan, A., Heyer, M.P., Ishikawa, M., Caligiuri, S.P.B., Liu, X.A., Chen, Z., Micioni Di Bonaventura, M.V., Elayouby, K.S., Ables, J.L., Howe, W.M., et al. (2019). Habenular TCF7L2 links nicotine addiction to diabetes. Nature *574*, 372–377. https://doi.org/10.1038/s41586-019-1653-x.

Filková, M., Aradi, B., Šenolt, L., Ospelt, C., Vettori, S., Mann, H., Filer, A., Raza, K., Buckley, C.D., Snow, M., et al. (2014). Association of circulating miR-223 and miR-16 with disease activity in patients with early rheumatoid arthritis. Ann. Rheum. Dis. *73*, 1898–1904. https://doi.org/10.1136/annrheumdis-2012-202815.

Fiorucci, S., Distrutti, E., Carino, A., Zampella, A., and Biagioli, M. (2021). Bile acids and their receptors in metabolic disorders. Prog. Lipid Res. *82*, 101094. https://doi.org/10.1016/j.plipres.2021.101094.

Grimaldi, A., Pietropaolo, G., Stabile, H., Kosta, A., Capuano, C., Gismondi, A., Santoni, A., Sciume, G., and Fionda, C. (2021). The regulatory activity of noncoding RNAs in ILCs. Cells *10*, 2742. https://doi.org/10.3390/cells10102742.

Gui, X., and Carraway, R.E. (2001). Enhancement of jejunal absorption of conjugated bile acid by neurotensin in rats. Gastroenterology *120*, 151–160. https://doi.org/10.1053/gast.2001.20876.

Guo, L., Qiu, Z., Wei, L., Yu, X., Gao, X., Jiang, S., Tian, H., Jiang, C., and Zhu, D. (2012). The MicroRNA-328 regulates hypoxic pulmonary hypertension by targeting at insulin growth factor 1 receptor and L-type calcium channel-α1C. Hypertension *59*, 1006–1013. https://doi.org/10.1161/hypertensionaha.111.185413.

Guo, X., Zhang, Z., Zeng, T., Lim, Y.C., Wang, Y., Xie, X., Yang, S., Huang, C., Xu, M., Tao, L., et al. (2019). cAMP-MicroRNA-203-IFNγ network regulates subcutaneous white fat browning and glucose tolerance. Mol. Metab. *28*, 36–47. https://doi.org/10.1016/j.molmet.2019.07.002.

Hasanzadeh, M., Movahedi, M., Rejali, M., Maleki, F., Moetamani-Ahmadi, M., Seifi, S., Hosseini, Z., Khazaei, M., Amerizadeh, F., Ferns, G.A., et al. (2019). The potential prognostic and therapeutic application of tissue and circulating microRNAs in cervical cancer. J. Cell. Physiol. *234*, 1289–1294. https://doi.org/10.1002/jcp.27160.

He, X., Kuang, G., Wu, Y., and Ou, C. (2021). Emerging roles of exosomal miRNAs in diabetes mellitus. Clin. Transl. Med. *11*, e468. https://doi.org/10.1002/ctm2.468.

Hofer, U. (2021). Unique bile acid metabolism in centenarians. Nat. Rev. Microbiol. *19*, 618. https://doi.org/10.1038/s41579-021-00623-7.

Hur, K., Toiyama, Y., Okugawa, Y., Ide, S., Imaoka, H., Boland, C.R., and Goel, A. (2017). Circulating microRNA-203 predicts prognosis and metastasis in human colorectal cancer. Gut *66*, 654–665. https://doi.org/10.1136/gutjnl-2014-308737.

Jang, Y., Je, Y.T., Yun, C.W., and Chung, H. (2017). Chitosan dosage regimen to trap fecal oil excretion after peroral lipase inhibitor administration in mice. Int. J. Biol. Macromol. *94*, 484–491. https://doi.org/10.1016/j.ijbiomac.2016.10.003.

Jiao, N., Baker, S.S., Chapa-Rodriguez, A., Liu, W., Nugent, C.A., Tsompana, M., Mastrandrea, L., Buck, M.J., Baker, R.D., Genco, R.J., et al. (2018). Suppressed hepatic bile acid signalling despite elevated production of primary and secondary bile acids in NAFLD. Gut *67*, 1881–1891. https://doi.org/10.1136/gutjnl-2017-314307.

Jimenez-Pascual, A., Hale, J.S., Kordowski, A., Pugh, J., Silver, D.J., Bayik, D., Roversi, G., Alban, T.J., Rao, S., Chen, R., et al. (2019). ADAMDEC1 maintains a growth factor signaling loop in cancer stem cells. Cancer Discov. *9*, 1574–1589. https://doi.org/10.1158/2159-8290.cd-18-1308.

Jin, Z.Q. (2021). MicroRNA targets and biomarker validation for diabetes-associated cardiac fibrosis. Pharmacol. Res. *174*, 105941. https://doi.org/10.1016/j.phrs.2021.105941.

Kim, H.J., Cho, H., Alexander, R., Patterson, H.C., Gu, M., Lo, K.A., Xu, D., Goh, V.J., Nguyen, L.N., Chai, X., et al. (2014). MicroRNAs are required for the feature maintenance and differentiation of brown adipocytes. Diabetes *63*, 4045–4056. https://doi.org/10.2337/db14-0466.

Kübeck, R., Bonet-Ripoll, C., Hoffmann, C., Walker, A., Müller, V.M., Schüppel, V.L., Lagkouvardos, I., Scholz, B., Engel, K.H., Daniel, H., et al. (2016). Dietary fat and gut microbiota interactions determine diet-induced obesity in mice. Mol. Metab. *5*, 1162–1174. https://doi.org/10.1016/j.molmet.2016.10.001.

Kunst, R.F., Verkade, H.J., Oude Elferink, R.P., and Graaf, S.F. (2021). Targeting the four pillars of enterohepatic bile salt cycling; lessons from genetics and pharmacology. Hepatology *73*, 2577–2585. https://doi.org/10.1002/hep.31651.

Kwekkeboom, R.J., Lei, Z., Doevendans, P., Musters, R., and Sluijter, J.G. (2014). Targeted delivery of miRNA therapeutics for cardiovascular diseases: opportunities and challenges. Clin. Sci. (Lond) *127*, 351–365. https://doi.org/10.1042/cs20140005.

Laanesoo, A., Urgard, E., Periyasamy, K., Laan, M., Bochkov, Y.A., Aab, A., Magilnick, N., Pooga, M., Gern, J.E., Johnston, S.L., et al. (2021). Dual role of the miR-146 family in rhinovirus-induced airway inflammation and allergic asthma exacerbation. Clin. Transl. Med. *11*, e427. https://doi.org/10.1002/ctm2.427.

Lei, S., Huang, F., Zhao, A., Chen, T., Chen, W., Xie, G., Zheng, X., Zhang, Y., Yu, H., Zhang, P., et al. (2017). The ratio of dihomo-gamma-linolenic acid to deoxycholic acid species is a potential biomarker for the metabolic abnormalities in obesity. FASEB J. *31*, 3904–3912. https://doi.org/10.1096/fj.201700055r.

Li, M., Wang, Q., Li, Y., Cao, S., Zhang, Y., Wang, Z., Liu, G., Li, J., and Gu, B. (2020). Apical sodium-dependent bile acid transporter, drug target for bile acid related diseases and delivery target for prodrugs: current and future challenges. Pharmacol. Ther. *212*, 107539. https://doi.org/10.1016/j.pharmthera.2020.107539.

Li, H., Zhang, N., Jiao, X., Wang, C., Sun, W., He, Y., Ren, G., Huang, S., Li, M., Chang, Y., et al. (2021a). Downregulation of microRNA-6125 promotes colorectal cancer growth through YTHDF2-dependent recognition of N6-methyladenosine-modified GSK3β. Clin. Transl. Med. *11*, e602. https://doi.org/10.1002/ctm2.602.

Li, H.M., Liu, X., Meng, Z.Y., Wang, L., Zhao, L.M., Chen, H., Wang, Z.X., Cui, H., Tang, X.Q., Li, X.H., et al. (2021b). Kanglexin delays heart aging by promoting mitophagy. Acta Pharmacol. Sin. *43*, 613–623. https://doi.org/10.1038/s41401-021-00686-5.

Lin, H., An, Y., Tang, H., and Wang, Y. (2019). Alterations of bile acids and gut microbiota in obesity induced by high fat diet in rat model. J. Agric. Food Chem. *67*, 3624–3632. https://doi.org/10.1021/acs.jafc.9b00249.

Lingvay, I., Sumithran, P., Cohen, R.V., and le Roux, C.W. (2021). Obesity management as a primary treatment goal for type 2 diabetes: time to reframe the conversation. Lancet *399*, 394–405. https://doi.org/10.1016/S0140-6736(21)01919-X.

Liu, G., Ye, Z., Zhao, X., and Ji, Z. (2017). SP1-induced up-regulation of lncRNA SNHG14 as a ceRNA promotes migration and invasion of clear cell renal cell carcinoma by regulating N-WASP. Am. J. Cancer Res. *7*, 2515–2525.

Mansour Aly, D., Dwivedi, O.P., Prasad, R.B., Käräjämäki, A., Hjort, R., Thangam, M., Åkerlund, M., Mahajan, A., Udler, M.S., Florez, J.C., et al. (2021). Genome-wide association analyses highlight etiological differences underlying newly defined subtypes of diabetes. Nat. Genet. *53*, 1534–1542. https://doi.org/10.1038/s41588-021-00948-2.

Marthaler, A.M., Podgorska, M., Feld, P., Fingerle, A., Knerr-Rupp, K., Grässer, F., Smola, H., Roemer, K., Ebert, E., Kim, Y.J., et al. (2017). Identification of C/EBPα as a novel target of the HPV8 E6 protein regulating miR-203 in human keratinocytes. PLoS Pathog. *13*, e1006406. https://doi.org/10.1371/journal.ppat.1006406.

Muraoka, T., Aoki, K., Iwasaki, T., Shinoda, K., Nakamura, A., Aburatani, H., Mori, S., Tokuyama, K., Kubota, N., Kadowaki, T., and Terauchi, Y. (2011). Ezetimibe decreases SREBP-1c expression in liver and reverses hepatic insulin resistance in mice fed a high-fat diet. Metabolism *60*, 617–628. https://doi.org/10.1016/j.metabol.2010.06.008.

Nakajima, A., Seki, M., Taniguchi, S., Ohta, A., Gillberg, P.G., Mattsson, J.P., and Camilleri, M. (2018). Safety and efficacy of elobixibat for chronic constipation: results from a randomised, double-blind, placebo-controlled, phase 3 trial and an open-label, single-arm, phase 3 trial. Lancet Gastroenterol. Hepatol. *3*, 537–547. https://doi.org/10.1016/s2468-1253(18)30123-7.

Nanfa, D., Sobngwi, E., Atogho-Tiedeu, B., Noubiap, J.J.N., Donfack, O.S., Mofo, E.P.M., Guewo-Fokeng, M., Nguimmo Metsadjio, A., Ndonwi Ngwa, E., Pokam Fosso, P., et al. (2015). Association between the TCF7L2 rs12255372 (G/T) gene polymorphism and type 2 diabetes mellitus in a Cameroonian population: a pilot study. Clin. Transl. Med. *4*, 17. https://doi.org/10.1186/s40169-015-0058-1.

Newsome, P.N., Palmer, M., Freilich, B., Sheikh, M.Y., Sheikh, A., Sarles, H., Herring, R., Mantry, P., Kayali, Z., Hassanein, T., et al. (2020). Volixibat in adults with non-alcoholic steatohepatitis: 24-week interim analysis from a randomized, phase II study. J. Hepatol. *73*, 231–240. https://doi.org/10.1016/j.jhep.2020.03.024.

Nie, B., Park, H.M., Kazantzis, M., Lin, M., Henkin, A., Ng, S., Song, S., Chen, Y., Tran, H., Lai, R., et al. (2012). Specific bile acids inhibit hepatic fatty acid uptake in mice. Hepatology *56*, 1300–1310. https://doi.org/10.1002/hep.25797.

Northey, J.J., Barrett, A.S., Acerbi, I., Hayward, M.K., Talamantes, S., Dean, I.S., Mouw, J.K., Ponik, S.M., Lakins, J.N., Huang, P.J., et al. (2020). Stiff stroma increases breast cancer risk by inducing the oncogene ZNF217. J. Clin. Invest. *130*, 5721–5737. https://doi.org/10.1172/jci129249.

Oteng, A.B., Higuchi, S., Banks, A.S., and Haeusler, R.A. (2021). Cyp2c-deficiency depletes muricholic acids and protects against high-fat diet-induced obesity in male mice but promotes liver damage. Mol. Metab. *53*, 101326. https://doi.org/10.1016/j.molmet.2021.101326.

Ovadia, C., Perdones-Montero, A., Spagou, K., Smith, A., Sarafian, M.H., Gomez-Romero, M., Bellafante, E., Clarke, L.C.D., Sadiq, F., Nikolova, V., et al. (2019). Enhanced microbial bile acid deconjugation and impaired ileal uptake in pregnancy repress intestinal regulation of bile acid synthesis. Hepatology *70*, 276–293. https://doi.org/10.1002/hep.30661.

Perino, A., Demagny, H., Velazquez-Villegas, L., and Schoonjans, K. (2021). Molecular physiology of bile acid signaling in health, disease, and aging. Physiol. Rev. *101*, 683–731. https://doi.org/10.1152/physrev.00049.2019.

Poupon, R. (2016). ASBT inhibitors in cholangiopathies - good for mice, good for men? J. Hepatol. *64*, 537–538. https://doi.org/10.1016/j.jhep.2015.12.007.

Pozzo, L., Vornoli, A., Coppola, I., Croce, C.M.D., Giorgetti, L., Gervasi, P.G., and Longo, V. (2016). Effect of HFD/STZ on expression of genes involved in lipid, cholesterol and glucose metabolism in rats. Life Sci. *166*, 149–156. https://doi.org/10.1016/j.lfs.2016.09.022.

Quante, M., Iske, J., Uehara, H., Minami, K., Nian, Y., Maenosono, R., Matsunaga, T., Liu, Y., Azuma, H., Perkins, D., Alegre, M.L., Zhou, H., Elkhal, A., and Tullius, S.G. (2021). Taurodeoxycholic acid and valine reverse obesity-associated augmented alloimmune responses and prolong allograft survival. Am. J. Transplant. *22*, 402–413. https://doi.org/10.1111/ajt.16856.

Rao, A., Kosters, A., Mells, J.E., Zhang, W., Setchell, K.D.R., Amanso, A.M., Wynn, G.M., Xu, T., Keller, B.T., Yin, H., et al. (2016). Inhibition of ileal bile acid uptake protects against nonalcoholic fatty liver disease in high-fat diet-fed mice. Sci. Transl. Med. *8*, 357ra122. https://doi.org/10.1126/scitranslmed.aaf4823.

Schattenberg, J.M., Pares, A., Kowdley, K.V., Heneghan, M.A., Caldwell, S., Pratt, D., Bonder, A., Hirschfield, G.M., Levy, C., Vierling, J., et al. (2021). A randomized placebo-controlled trial of elafibranor in patients with primary biliary cholangitis and incomplete response to UDCA. J. Hepatol. *74*, 1344–1354. https://doi.org/10.1016/j.jhep.2021.01.013.

Singh, A.K., Chaube, B., Zhang, X., Sun, J., Citrin, K.M., Canfrán-Duque, A., Aryal, B., Rotllan, N., Varela, L., Lee, R.G., et al. (2021). Hepatocyte-specific suppression of ANGPTL4 improves obesity-associated diabetes and mitigates atherosclerosis in mice. J. Clin. Invest. *131*, e140989. https://doi.org/10.1172/JCI140989.

Sundaram, S., Palaniappan, B., Nepal, N., Chaffins, S., Sundaram, U., and Arthur, S. (2019). Mechanism of dyslipidemia in obesity-unique regulation of ileal villus cell brush border membrane sodium-bile acid cotransport. Cells *8*, 1197. https://doi.org/10.3390/cells8101197.

Swarup, V., Hinz, F.I., Rexach, J.E., Noguchi, K.I., Toyoshiba, H., Oda, A., Hirai, K., Sarkar, A., Seyfried, N.T., Cheng, C., et al. (2019). Identification of evolutionarily conserved gene networks mediating neurodegenerative dementia. Nat. Med. *25*, 152–164. https://doi.org/10.1038/s41591-018-0223-3.

Ting, W., Feng, C., Zhang, M., Long, F., and Bai, M. (2020). RETRACTED: overexpression of microRNA-203 suppresses proliferation, invasion, and migration while accelerating apoptosis of CSCC cell line SCL-1. Mol. Ther. Nucleic Acids *21*, 428–440. https://doi.org/10.1016/j.omtn.2020.04.014.

Trampert, D.C., van de Graaf, S.F., Jongejan, A., Oude Elferink, R.P., and Beuers, U. (2021). Hepatobiliary acid-base homeostasis: insights from analogous secretory epithelia. J. Hepatol. *74*, 428–441. https://doi.org/10.1016/j.jhep.2020.10.010.

Treiber, T., Treiber, N., and Meister, G. (2019). Regulation of microRNA biogenesis and its crosstalk with other cellular pathways. Nat. Rev.

Mol. Cell Biol. *20*, 5–20. https://doi.org/10.1038/s41580-018-0059-1.

Tysoe, O. (2021). Adipocytes enter the cell cycle in obesity. Nat. Rev. Endocrinol. *17*, 705. https://doi.org/10.1038/s41574-021-00589-9.

van de Peppel, I.P., Rao, A., Dommerholt, M.B., Bongiovanni, L., Thomas, R., de Bruin, A., Karpen, S.J., Dawson, P.A., Verkade, H.J., and Jonker, J.W. (2020). The beneficial effects of apical sodium-dependent bile acid transporter inactivation depend on dietary fat composition. Mol. Nutr. Food Res. *64*, e2000750. https://doi.org/10.1002/mnfr.202000750.

Wang, L., Wang, B., Gasek, N.S., Zhou, Y., Cohn, R.L., Martin, D.E., Zuo, W., Flynn, W.F., Guo, C., Jellison, E.R., Kim, T., et al. (2021). Targeting p21(Cip1) highly expressing cells in adipose tissue alleviates insulin resistance in obesity. Cell Metab. *34*, 186. https://doi.org/10.1016/j.cmet.2021.12.014.

Wu, Q., Liang, X., Wang, K., Lin, J., Wang, X., Wang, P., Zhang, Y., Nie, Q., Liu, H., Zhang, Z., et al. (2021). Intestinal hypoxia-inducible factor 2α regulates lactate levels to shape the gut microbiome and alter thermogenesis. Cell Metab. *33*, 1988–2003.e7. https://doi.org/10.1016/j.cmet.2021.07.007.

Yang, X., Li, J., Zhao, L., Chen, Y., Cui, Z., Xu, T., Li, X., Wu, S., and Zhang, Y. (2021). Targeting adipocytic discoidin domain receptor 2 impedes fat gain while increasing bone mass. Cell Death Differ. *29*, 737–749. https://doi.org/10.1038/s41418-021-00887-9.

Yoshimoto, S., Loo, T.M., Atarashi, K., Kanda, H., Sato, S., Oyadomari, S., Iwakura, Y., Oshima, K., Morita, H., Hattori, M., et al. (2013). Obesity-induced gut microbial metabolite promotes liver cancer through senescence secretome. Nature *499*, 97–101. https://doi.org/10.1038/nature12347.

Zamek-Gliszczynski, M.J., Kenworthy, D., Bershas, D.A., Sanghvi, M., Pereira, A.I., Mudunuru, J., Crossman, L., Pirhalla, J.L., Thorpe, K.M., Dennison, J.M., et al. (2021). Pharmacokinetics and ADME characterization of intravenous and oral [(14)C]-linerixibat in healthy male volunteers. Drug Metab. Dispos. *49*, 1109–1117. https://doi.org/10.1124/dmd.121.000595.

Zhang, S.Y., Li, R.J.W., Lim, Y.M., Batchuluun, B., Liu, H., Waise, T.M.Z., and Lam, T.K.T. (2021a). FXR in the dorsal vagal complex is sufficient and necessary for upper small intestinal microbiome-mediated changes of TCDCA to alter insulin action in rats. Gut *70*, 1675–1683. https://doi.org/10.1136/gutjnl-2020-321757.

Zhang, Y., Liu, J., Mao, G., Zuo, J., Li, S., Yang, Y., Thring, R.W., Wu, M., and Tong, H. (2021b). Sargassum fusiforme fucoidan alleviates diet-induced insulin resistance by inhibiting colon-derived ceramide biosynthesis. Food Funct. *12*, 8440–8453. https://doi.org/10.1039/d1fo01272j.

STAR★METHODS

KEY RESOURCES TABLE

REAGENT or RESOURCE	SOURCE	IDENTIFIER
Antibodies		
Anti-ASBT	Abcam	Cat# ab203205 (1:1000 dilution); RRID: AB_2801376
Anti-TCF7L2	Bioss	Cat# bs-1280R (1:500 dilution); RRID: AB_10855768
Anti-ASBT	Santa Cruz Biotechnology	Cat# sc-27493 (1:250 dilution); RRID: AB_2188364
Anti-TCF7L2	Abcam	Cat# ab76151 (1:200 dilution); RRID: AB_1310728
Anti-GAPDH	OriGene	Cat# TA802519 (1:1000 dilution); RRID: AB_2626378
Biological samples		
Human cecum samples	the Second Affiliated Hospital of Harbin Medical University	N/A
Human plasma samples	the Second Affiliated Hospital of Harbin Medical University	N/A
Chemicals, peptides, and recombinant proteins		
TRIzol RNA isolation reagent	Thermo Fisher Scientific	Cat#15596026
RIPA buffer	Sularbio	Cat#r0010
high fat diet	Huafukang Biological Technology	Cat#10045
High-Capacity cDNA Reverse Transcription Kit	Toyobo	Cat#fsq-101
SYBR Green I	Toyobo	Cat#qps-201
paraformaldehyde	Sigma	Cat#t81108
Triton X-100	Sularbio	Cat#t8200
Opti-MEM	Invitrogen	Cat#31985070
X-tremeGENE HP DNA transfection reagent	Sigma	Cat#4476115001
Protease Inhibitor Cocktail	Shennengbocai	Cat#P1003
DAPI	beyotime	Cat#c1002
Nuclear and cytoplasmic Extraction Reagents	Thermo Fisher Scientific	Cat# 78833
Critical commercial assays		
LDL-C ELISA assay kit	Nanjing Jiancheng Biotech	Cat# A113-1-1
HDL-C ELISA assay kit	Nanjing Jiancheng Biotech	Cat# A112-1-1
TG ELISA assay kit	Nanjing Jiancheng Biotech	Cat# A110-1-1
TC ELISA assay kit	Nanjing Jiancheng Biotech	Cat# F002-1-1
Total bile acid assay kit	Nanjing Jiancheng Biotech	Cat# E003-1-1
TAGs assay kit	Abbkine	Cat# KTB2200
NEFA assay kit	Elabscience	Cat# E-BC-K013-S
ChIP assay kit	Thermo Fisher Scientific	Cat# 26156
EMSA Kit	Thermo Fisher Scientific	Cat# 20148
Experimental models: Cell lines		
HIEC cell line	ATCC	Cat# CCL-241
HEK293 cell line	ATCC	Cat# CRL-11268
Experimental models: Organisms/strains		
Mouse: WT C57BL/6JNifdc	Charles River Laboratories	Cat# 219
RAT: WT SD	Charles River Laboratories	Cat# 101

(*Continued on next page*)

Continued

REAGENT or RESOURCE	SOURCE	IDENTIFIER
Software and algorithms		
Prism	Graphpad	https://www.graphpad.com/scientific-software/prism/
ImageJ	NIH	https://imagej.nih.gov/ij/

RESOURCE AVAILABILITY

Lead contact

Further information and requests for resources and reagents should be directly to and will be fulfilled by the Lead Contact, Yong Zhang (hmuzhangyong@hotmail.com).

Materials availability

This study did not generate new unique reagents. Materials generated in this study is available from the lead contact upon request.

Data and code availability

Data reported in this paper will be shared by the lead contact upon request. This paper does not report original code. Any additional information required to reanalyze the data reported in this paper is available from the lead contact upon request.

EXPERIMENTAL MODEL AND SUBJECT DETAILS

Study approval

The protocols of this study were approved by the Ethics and Scientific Committees of Harbin Medical University (Harbin, China). Written informed consents were obtained from all the enrolled patients (HMUIRB20170018). The experimental procedures were performed in accordance with the Guide for the Care and Use of Laboratory Animals, published by the US National Institutes of Health (NIH Publication No. 85e23, revised 1996).

Obese rat model

8-week-old male SD rats weighting 150 $\pm$ 10 g (SPF grade, Second Affiliated Hospital of Harbin Medical University Experimental Animal Center) were housed in light and dark cycle of 12 h, 50% humidity, and at 25 $\pm$ 2°C. The rats were randomly divided into five groups (n = 6): lean rats (control group), obese rats (obesity group), obese rats with agomiR-203 administration (agomiR-203 group); obese rats with antagomiR-203 administration group (antagomiR-203 group); obese rats with negative control administration (negative control group). The lean rats were treated with standard diet and obese rats were given high fat diet for four weeks. Food and water were given *ad libitum*. The high fat diet (45% kcal as fat) is purchased from Huafukang Biological Technology (10045). At the second week, we injected experimental reagents into the ileocolon artery mesentery of rats after abdominal operation according to experimental designs of every group. The rats were anesthetized with pentobarbital sodium and placed in the supine position with the upper limbs taped to the table. A 1-1.5 cm incision was made along the left side of the hypogastric zone. The muscle layers were bluntly dissected and the peritoneum was cut open. The cecum was pulled out slightly and covered by sterile gauze saddened with physiological saline. AgomiR-203 (0.5 nmol), antagomiR-203 (0.5 nmol) and NC (0.5 nmol) solutions were injected into ileocolon artery mesentery. All surgical procedures were performed under sterile conditions. At the start of third week and forth week, we directly injected the same dose of reagents into abdominal cavity of each group. Body weight of rats in different groups was measured each week. At the end of forth week, the rats were fasted for 12 h. 3% pentobarbital sodium (0.2 mL/100 g) was injected into abdominal cavity for anesthesia. 3 to 5 mL of abdominal aortic blood was collected and centrifugated at 2500 rpm for 8 min to separate serum. Periepididymal fat were taken and weighted. Terminal ileum about 6 cm long were separated for further detection. AgomiR, antagomiR and NC sequences are shown in Table S1.

MiR-203 overexpression transgenic mice

The miR-203 overexpression transgenic mice were generated as previously described (Guo et al., 2012). Briefly, the vector containing pre-miR-203 sequence was constructed by recombinant DNA technology. The DNA fragment containing the pre-miR-203 sequence was prepared after digestion, separation and purification. Eggs from sexually post-mated female mice (C57BL/6, 2 months, 20 ± 3 g) were microinjected with the DNA fragment individually. Then implanting the injected eggs into the pseudopregnant female mice. Genomic DNA was isolated and detected for the successful transgene presence by PCR analysis. 2-month-old wild-type (WT) C57BL/6 mice and 2-month-old TgN (miR-203) mice (20 ± 3 g) were randomly selected and divided into the following groups: wild-type mice treated with normal diet (WT-ND); wild-type mice treated with high-fat diet (WT-HFD); transgenic mice treated with normal diet (TgN (miR-203)-ND) and high-fat diet (TgN (miR-203)-HFD); TgN (miR-203) mice injected with antagomiR-203 (TgN (miR-203)-HFD + ant) and negative control reagent (TgN (miR-203)-HFD + NC) on the basis of HFD. 0.5 nmol reagents were injected intraperitoneally once a week. The body weight was weighed every week. At the end of the ninth week, after anesthesia, the fat distribution of mice in each group was examined by positron emission tomography-computed tomography (PET-CT), and the mice were photographed. The periepididymal fat of mice in each group were separated for weighing, and the terminal ileum and abdominal aortic blood were taken for further experiments.

HIEC cell line

The HIEC (Human intestinal epithelial cell) cell line (CCL-241) was purchased from ATCC and cultured in matched Hybri-Care Medium (46-X, ATCC) containing 30 ng/mL epidermal growth factor, 1% penicillin/streptomycin and 10% fetal bovine serum. The cells were isolated from the small intestine of a 3 to 4 months gestation, female patient. Maintaining the cells in the condition of 5% CO_2 and 95% air at 37°C.

Human samples

The human cecum samples were obtained from 60 enrolled patients (Age: 42 ± 12 yrs; gender: 33 (55%) male) who received endoscopic polypectomy in the Second Affiliated Hospital of Harbin Medical University between January 2017 and January 2018. 105 patients (Age: 48 ± 14 yrs; gender: 42 (40%) male) who received physical examination at the Second Affiliated Hospital of Harbin Medical University between January 2017 and January 2018 were enrolled for plasma collection. Participants were excluded for the following standards: prevalent hypertension (SBP ≥140 mmHg, DBP ≥90 mmHg; diabetes mellitus (fasting glucose ≥126 mg/dL); history of CVD (coronary artery disease, heart arrhythmia, myocardial infarction, cerebral hemorrhage and heart failure); history of cancer.

METHOD DETAILS

Measurement of serum lipid and total bile acid

Serum low-density lipoprotein cholesterol (LDL-C) (A113-1-1, Nanjing Jiancheng Biotech), serum high-density lipoprotein cholesterol (HDL-C) (A112-1-1, Nanjing Jiancheng Biotech), serum and fecal total cholesterol (TCH) (F002-1-1, Nanjing Jiancheng Biotech), serum and fecal triglyceride (TG) (A110-1-1, Nanjing Jiancheng Biotech), serum and fecal total bile acid (TBA) (E003-1-1, Nanjing Jiancheng Biotech) were measured with corresponding assay kits. The experimental procedure was performed according to the manufacturer's instructions.

Measurement of serum bile acid profile

The bile acid standards were obtained from Steraloids Inc. (Newport, RI, USA), TRC Chemicals (Toronto) and C/D/N Isotopes Inc. Internal standards were used to keep data quality and correct for matrix effects. 180 μL acetonitrile/methanol (8:2) (including 10 internal standards) was added to 20 μL serum samples in a 96-well plate and metabolites were extracted by shaking at 1500 rpm for 20 min at 10°C. After centrifugation, transfer the supernatant to a microcentrifuge tube and lyophilize using a FreeZone lyophilizer equipped with a parking system (Labconco). After that, dry powder, lyophilized calibrator and BAP Ultra QC samples were collected and transferred to 96-well plates for LC-MS analysis. Bile acids were determined by liquid chromatography (tacem-tandem mass spectrometry (UPLC-MS/MS)) (ACQUITY UPLC-Xevo TQ-S).

Fat tolerance test

Fat tolerance test was performed based on previous study (Singh et al., 2021). Briefly, After a 4-h fast, mice were administered with olive oil by oral gavage at 10 μL/g of body weight. Blood samples were collected

from the orbit after 0, 1, 2, and 4 h oral gavage. Plasma TAGs (KTB2200, Abbkine) and NEFA (E-BC-K013-S, Elabscience) were measured using Colorimetric Assay Kit.

RNA extraction and quantitative real-time PCR

Total RNA was extracted in accordance with the liquid nitrogen Trizol (15596026, Thermo Fisher Scientific) one-step method from serum, tissues and cells. After reverse transcription with High-Capacity cDNA Reverse Transcription Kit (fsq-101, Toyobo), the expression levels of RNAs were detected by SYBR Green I (qps-201, Toyobo) and calculated as values of $2^{-\Delta\Delta Ct}$. GAPDH and U6 was used as internal control. Primers used were shown in Table S1.

Western blot

Western blot analysis was performed as described previously (Li et al., 2021b). Briefly, lyse the tissues and cells in RIPA buffer (r0010, Sularbio) containing protease inhibitors (P1003, Shennengbocai). 60-80 μg protein samples were loaded on a 10% SDS-PAGE gel and transferred to nitrocellulose membranes. The membranes were blocked in the 5% non-fat milk PBS solution for 2 h. Primary antibodies including ASBT (sc-27493, Santa Cruz Biotechnology) and TCF7L2 (bs-1280R, Bioss) were incubated for 12 h at 4°C. GAPDH and actin were used as an internal control (TA802519, OriGene). Secondary antibodies were incubated for 2 h at room temperature,. The target bands were analysed using Odyssey Infrared Imaging System (LI-COR).

Immunofluorescence

Frozen sections of cecum were fixed with 4% paraformaldehyde (t81108, Sigma) for 30 min at room temperature, and then penetrated with 0.6% Triton X-100 (t8200, Sularbio) for 1 h. Subsequently, tissue sections were blocked by goat serum for 30 min and incubated with anti-ASBT primary antibody (ab203205, Abcam) at 4°C for 12 h. After that, the sections were incubated with fluorophore-labeled secondary antibodies (Invitrogen) for 1 h. DAPI (c1002, beyotime) was used to label nucleus. Fluorescence was examined under a confocal laser scanning microscope (Nikon 80i).

Luciferase reporter assay

Construction of luciferase-miRNA-target site fusion plasmids: Luciferase reporters containing wild-type or mutated 3′UTR of SLC10A2 plasmid were constructed using psi-CHECK2 vectors (Promega). The luciferase vector (100 ng) was co-transfected with miR-203 mimic, miR-203 AMO, or negative control (scramble sequence of miR-203) into human embryonic kidney 293 (HEK293) cells (CRL-11268, ATCC). Renilla luciferase reporters were used as an internal control. After 48 h, the cells were collected and lysed. Luciferase activities were examined by Dual-Luciferase Reporter Assay System (Promega). Construction of promoter-luciferase fusion plasmids: Fragments that containing the TCF7L2-binding sites in miR-203 promoter were synthesized (Invitrogen). The fragments were subcloned into luciferase-containing pGL3-promoter vector (Promega) for investigating the role of TCF7L2 in promoting transcription of the miR-203. Oligonucleotides used were shown in Table S1.

dODNs synthesis

Single-chain phosphorothioate dODN was synthesized by Integrated DNA Technologies. Dissolve the ODN in sterilized Tris-EDTA buffer. The supernatant was purified and quantified by spectrophotometry. Then, the complementary single-stranded ODN was heated to 95°C for 10 min, and then slowly cooled to room temperature over 2 h to generate double-stranded dODN. The dODN was dissolved in saline at a final concentration of 50 μM. A scrambled dODN was also used as internal control.

Cell transfection

HIECs was transfected with miR-203 mimic, miR-203 AMOs and negative control respectively (RiboBio). The transfection reagents was added into Opti-MEM (31985070, Invitrogen) serum-free medium (100 nM) and transfected into HIECs using X-treme reagent (4476115001, Sigma). Cells were harvested 48 h after transfection to extract total RNA or protein. Transfection reagents and X-treme were separately mixed with 25 μL of Opti-MEM. Then blend the two mixtures and incubate for 20 min at room temperature. The mixture was added to the cells and incubated at 37°C for 5 h. Oligonucleotides for transfection are shown in Table S1.

ChIP assay

ChIP assay were conducted with the Thermo ChIP Kit (26156, Thermo Fisher Scientific). Briefly, HIECs were fixed in 1% formaldehyde for 10 min and nucleoprotein complexes were cross-linked. The pelleted cells were then lysed and sonicated with detergent lysis buffer. The lysate was incubated with 2 μg of anti-TCF7L2 antibody (ab76151, Abcam) to immunoprecipitate cleaved DNA-protein complexes. IgG was used as a controlt. Magnetic Protein G beads provided in Kit were used. After extensive washing, cross-links were removed by shaking with 100 μL ChIP Elution Buffer and 1 μL Protinase K for 2 h, and DNA was isolated using the QIAquick PCR Purification Kit (QIAGEN). The existance of the miR-203 promoter was analyzed by PCR amplification. Analyze PCR products by 1% agarose gel electrophoresis using GelRed Nucleic Acid Gel Stain. Primers used were shown in Table S1.

EMSA

EMSA was performed with the LightShift® Chemiluminescent EMSA Kit (20148, Thermo Fisher Scientific). Nuclear protein extracts from HIECs using Nuclear and cytoplasmic Extraction Reagents (78833, Thermo Fisher Scientific) and were incubated with DIG-labeled double stranded oligonucleotides containing the putative TCF7L2 *cis*-acting element. For competition experiments, 500-fold excess of unlabeled double-stranded TCF7L2 consensus oligonucleotides. Mutant probe was also synthesized for experiment. For super-shift experiments, 1 μg of TCF7L2 antibody (ab76151, Abcam) were added to the reaction. The generated chemiluminescent signals were recorded on x-ray film. Probe sequences were provided in Table S1.

QUANTIFICATION AND STATISTICAL ANALYSIS

The experiments was randomized and blinded. All data were presented as the mean ± SEM. Statistical comparisons between the two groups were performed using Student's t-test. Differences among multiple groups were analyzed by one-way ANOVA with Turkey's Multiple Comparison Test (GraphPad Prism 8.3.0). Data of clinical samples were analyzed using the Kruskal-Wallis H and the Mann-Whitney U test by SPSS 19.0. $p < 0.05$ was considered statistically significant.